Food Hydrocolloids 172 (2026) 112163

Contents lists available at ScienceDirect

Food Hydrocolloids

journal homepage: www.elsevier.com/locate/foodhyd

Whey protein-based aerogels: Structural insights, zinc-carrier properties, and zinc bioavailability in Caco-2 cells

Helena Kieserling [a], Jonathan Heine [a,b], Baldur Schroeter [c], Stephan Drusch [d], Maria Maares [e], Sascha Rohn [a], Hajo Haase [b], Pavel Gurikov [c,f], Claudia Keil [b,*]

[a] Department of Food Chemistry and Analysis, Institute of Food Technology and Food Chemistry, Technische Universität Berlin, Kaiserin-Augusta-Allee 14, 10553, Berlin, Germany
[b] Department of Food Chemistry and Toxicology, Institute of Food Technology and Food Chemistry, Technische Universität Berlin, Kaiserin-Augusta-Allee 14, 10553, Berlin, Germany
[c] Laboratory for Development and Modelling of Novel Nanoporous Materials, Hamburg University of Technology, Eißendorfer Straße 38, 21073, Hamburg, Germany
[d] Department of Food Technology and Food Material Science, Institute of Food Technology and Food Chemistry, Technische Universität Berlin, Königin-Luise-Str. 22, 14195, Berlin, Germany
[e] Department of Food Chemistry, Institute of Nutritional Science, University of Potsdam, Arthur-Scheunert-Allee 114–116, 14558, Nuthetal, Germany
[f] Aerogel-it GmbH, Albert-Einstein-Str. 1, 49076, Osnabrück, Germany

ARTICLE INFO

Keywords:
Whey protein-based aerogels
Ion retention
Structural characterization
Digestibility
Zinc bioavailability

ABSTRACT

Due to their large surface area and modifiable structures, aerogels derived from biopolymers like whey protein isolate (WPI) are gaining attention as micronutrient carriers. However, their ability to incorporate essential trace elements like zinc, and how these ions affect aerogel structure and zinc bioavailability, remain poorly understood. This study aimed at characterizing the influence of zinc ions on the structural and morphological properties of WPI-based aerogels along with their ability for zinc delivery. Initially, hydrogels were prepared with WPI and zinc chloride at pH 1 and pH 3 and compared with formulations containing calcium chloride or sodium chloride. The hydrogels were then converted into aerogels via solvent exchange and supercritical drying. Analytical characterization included liquid chromatography-mass spectrometry for protein component profiling, flame atomic absorption spectrometry for metal retention, Fourier-transform infrared spectroscopy for secondary structure analysis, Brunauer-Emmett-Teller surface area measurements, scanning electron microscopy for morphological assessment, digestibility and zinc uptake in Caco-2 enterocytes via Zinpyr-1 fluorescence. Results showed a relative increase of β-lactoglobulin and a substantial ion loss during the hydrogel-to-alcogel transition – up to 70 % for calcium and 52 % for zinc – mainly due to solvent exchange, which affects protein-ion interactions. Fourier-transform infrared spectroscopy revealed increased intermolecular β-sheet formation and hydrogen bonding in the presence of divalent ions, suggesting enhanced protein-metal coordination. At pH 1, the aerogels exhibited pronounced porosity, a large surface area and enhanced enzymatic digestibility. In contrast, aerogels formed at pH 3 appeared denser, less digestible and retained higher amounts of metal ions. Zinc release from undigested aerogels was limited, likely due to matrix binding, whereas trypsin digestion slightly increased the zinc but without clear evidence for increased bioavailability compared to inorganic zinc. These findings show that pH and ion type influence the structure and function of WPI aerogels, highlighting their potential for targeted, digestible metal ion delivery.

1. Introduction

Aerogels represent a distinct class of materials characterized by low density, high porosity, and large surface area, rendering them highly suitable for a wide range of scientific and industrial applications. Aerogels are produced through a sol-gel process involving hydrogel formation, solvent exchange, and supercritical drying (Kistler, 1931). This process generally includes four key stages: (i) dissolution of the precursor material in an aqueous medium, (ii) gelation through (physico-)chemical interactions, (iii) replacement of water with an organic

* Corresponding author.
E-mail address: c.keil@tu-berlin.de (C. Keil).

https://doi.org/10.1016/j.foodhyd.2025.112163
Received 15 July 2025; Received in revised form 2 October 2025; Accepted 22 October 2025
Available online 23 October 2025

solvent like ethanol, and (iv) solvent removal by supercritical or ambient pressure drying to preserve a porous aerogel structure (Andlinger et al., 2021). Over the past decades, aerogels were predominantly produced from inorganic precursor materials such as silica, carbon and polyurethane, and utilized in various applications, including environmental and industrial fields (Smirnova & Gurikov, 2018). However, recent advancements focused on the development of biopolymer-based aerogels, particularly those made from proteins, for expanding their applicability in biomedicine and foods/feeds (Betz et al., 2012; Leite et al., 2025; Selvasekaran & Chidambaram, 2021; Wang, Li, et al., 2024). Hence, these protein-based aerogels can be obtained as stable, lightweight, and porous solids that may be directly consumed or integrated into novel food formats, thereby offering additional functional opportunities.

Globular proteins such as whey or egg proteins are particularly suitable as precursor materials to produce for instance temperature-induced hydrogels (Nicolai, 2019). During temperature-induced gelation, globular proteins undergo partial unfolding due to the disruption of intra- and intermolecular interactions, affecting their secondary, tertiary and quaternary structure. This unfolding exposes previously buried structural features, facilitating the formation of new intermolecular interactions. These include non-covalent interactions, such as hydrophobic and electrostatic interactions, hydrogen bonds, as well as covalent bonds in the presence of, e.g., cysteine residues (Rodrigues et al., 2015). As a result, proteins aggregate and form a three-dimensional network, leading to gel formation (Lorenzen & Schrader, 2006). The gelation process is highly pH-dependent, as the protonation state of selected protein side chains modulates electrostatic interactions, thereby influencing aggregation behavior and network structure. At the isoelectric point, the absence of electrostatic repulsion promotes aggregation, leading to the formation of dense, low-porosity particulate networks (Kleemann et al., 2018). In contrast, shifting the pH above or below the isoelectric point increases electrostatic repulsion, favoring the formation of string-like aggregates. These structures are essential for developing highly porous aerogels with small pore sizes and, consequently, a large surface area.

During the solvent exchange with ethanol, the balance of intra- and intermolecular interactions shifts, enhancing protein-protein interactions and thus, promoting structural rearrangements, ultimately leading to alcogel formation (Kleemann et al., 2018; Kleemann et al., 2020). In the subsequent stage, supercritical drying removes the solvent while preserving the porous network of the alcogel and resulting in protein-based aerogels. Whereas previous research on protein-based aerogels primarily focused on characterizing microstructure, such as specific surface area, porosity, and pore size (Betz et al., 2012; Lovskaya et al., 2022), the influence of the early gelation stages on the final aerogel structure remains insufficiently understood and has not been systematically clarified.

The large surface area and porosity of protein-based aerogels render them particularly suitable as carrier systems for bioactive compounds (Manzocco et al., 2021; Wang et al., 2024), including micronutrients such as essential metal ions. Among these, zinc is indispensable to human health, fulfilling catalytic, structural, and regulatory roles that sustain enzyme function, immune defense, cellular growth, as well as neurological and reproduction processes (Maret, 2017; Rink & Gabriel, 2000). Globally, zinc deficiency is recognized as a substantial public health problem, with 17.3 % of the world's population at risk because of inadequate intake (Wessells & Brown, 2012). Addressing this widespread deficiency will require the implementation of improved, forward-thinking zinc nutrition programs (Lowe et al., 2024). However, the bioavailability of zinc is influenced by dietary composition and physiological factors (Hall & King, 2023; Maares & Haase, 2020), emphasizing the need for advanced matrices that can enhance its bioaccessibility and absorption within the gastrointestinal tract. Here, protein-based materials – including aerogels – are emerging as effective zinc delivery platforms due to their zinc-binding affinity and enzymatic degradability, which may enhance intestinal absorption. As an example, whey protein hydrolysis during digestion can generate zinc-binding peptides, which may form bioavailable zinc-peptide complexes. Such peptide complexes have been shown to enhance zinc absorption, as reported by Peng et al. (2022) and Liu et al. (2022), potentially accounting for the increased zinc uptake observed in zinc-loaded protein-based aerogel digests.

Previous studies incorporated metal ions by altering ionic strength to modify aerogel characteristics, such as mechanical stability and textural properties. For instance, the addition of monovalent (e.g., Na^{+}) and divalent (e.g., Ca^{2+}) ions to the initial protein solutions has been shown to decrease the specific surface area of the final protein-based aerogels (Kleemann et al., 2018; Selmer et al., 2015). This effect was attributed to the ions' ability to screen charges, which reduces electrostatic interactions between protein molecules, resulting in the formation of less stable gel networks and subsequent alterations in pore structure. In contrast, several studies demonstrated that stable *no-salt-added* aerogels exhibit very high specific surface areas and mesoporosity (Andlinger et al., 2022; Jung et al., 2023; Plazzotta et al., 2021; Schroeter et al., 2021). However, it remains unclear whether ion-induced structural changes still allow for sufficient loading capacity and controlled release performance – an aspect that has not been systematically addressed. To date, metal ion incorporation has been primarily investigated for its influence on hydrogel formation and the resulting aerogel properties rather than its potential for bioactive metal ion delivery. However, no systematic studies assessed the suitability of protein-based aerogels as carrier systems for metal ions so far, leaving a gap in understanding their ion-binding capacity and controlled release behavior in duodenal fluid environments and their potential for cellular uptake. Moreover, there is a lack of data regarding how enterocytes manage zinc released from digested proteins or if this zinc is suitable for cellular absorption. Aerogels might provide an improved zinc release, depending on their structure formation.

Consequently, this study aimed at characterizing the structural and morphological properties of protein-based aerogels, as well as their zinc incorporation and bioavailability using the well characterized *in vitro* Caco-2 cell model. For this purpose, temperature-induced aerogels from whey protein isolate (WPI) were used as a model system and prepared at low initial pH. The low pH ensured to remain below the isoelectric point of the main protein fractions β-lactoglobulin (β-LG), α-lactalbumin (α-LA), and bovine serum albumin (BSA), while also creating a sufficiently acidic environment to prevent the formation of zinc hydroxide, which would otherwise limit zinc solubility and thus, bioavailability (Einhorn et al., 2024). Specifically, aerogels were produced at pH 1 and pH 3 with incorporated zinc chloride and compared to those containing other divalent ions (i.e., calcium chloride) and monovalent ions (i.e., sodium chloride) as controls. Regarding ion retention, it was hypothesized that aerogels prepared at pH 1 would exhibit lower calcium and zinc retention compared to those at pH 3 due to the higher protonation of the proteins' functional groups at pH 1, resulting in a highly positive net charge on the protein matrix. This increased positive charge would lead to enhanced electrostatic repulsion of the positively charged metal ions. With respect to aerogel structure, it was hypothesized that the presence of divalent metal ions would influence the hydrogen bonding pattern and promote structural modifications, potentially enhanced intermolecular β-sheet formation, due to their stronger interactions with the protein matrix and potential to form ionic bridges, compared to monovalent ions like sodium. It was further anticipated that denser aerogels formed at pH 3 would be less susceptible to proteolytic digestion, while the higher porosity at pH 1, due to increased electrostatic repulsion between protein strands, would enhance enzymatic accessibility. Finally, it was hypothesized that proteolytic digestion of the aerogels affects zinc delivery to enterocytes, potentially offering insights into the zinc aerogel's release mechanisms and its cell availability.

To test the hypotheses, a targeted proteomics approach using liquid chromatography-mass spectrometry (LC-MS) was employed to quantify

protein fractions throughout the aerogel preparation process. The amounts of calcium and zinc were determined using flame atomic absorption spectrometry (FAAS). The secondary structure of the aerogels was analyzed using Fourier-transform-infrared spectroscopy (FTIR). The surface and morphological properties of the aerogels were characterized by Brunauer-Emmett-Teller (BET) surface area analysis and scanning electron microscopy (SEM). Before cellular investigations, the aerogels were subjected to tryptic digestion as a model proteolysis step, and hydrolysis was monitored using sodium dodecyl sulfate-polyacrylamide gel electrophoresis (SDS-PAGE). Finally, a Caco-2 cell Zinpyr-1-based fluorimetric microassay was performed to assess the cellular availability of zinc upon applications of predigested aerogel samples.

2. Materials and methods

2.1. Preparation of aerogels

The preparation of zinc- and calcium-containing WPI aerogels followed the procedures described earlier (Betz et al., 2012; Kleemann et al., 2018). The aerogel preparation process usually comprises five steps: (i) preparation of aqueous whey protein solutions (BiPRO® 9500, Agropur, Montreal, Canada) with a constant protein concentration of 15 g/100 g and a pH value of either 1 or 3; (ii) addition of calcium and zinc ions in the form of $CaCl_2$ and $ZnCl_2$, respectively; (iii) thermally induced gelation; (iv) solvent exchange from water to ethanol; and (v) supercritical CO_2 ($scCO_2$) drying. For zinc-loaded aerogels, WPI solutions with 15 g protein per 100 g distilled water were prepared. $ZnCl_2$ (≥97 %, p.a., Carl Roth GmbH, Karlsruhe, Germany) was added to obtain different concentrations (50 mM, 100 mM, 200 mM $ZnCl_2$), and the pH was adjusted to 1 or 3 using 32 % hydrochloric acid. $ZnCl_2$, NaCl (≥99,5 %, p.a., Merck KGaA, Darmstadt, Germany), and WPI were weighed and dissolved in 90 g distilled water under stirring for 20 min to ensure complete dissolution. NaCl was added to maintain a constant ionic strength of 600 mM across all solutions, allowing the effect of zinc concentration on the final aerogel properties to be evaluated independently of ionic strength variations. Specifically, for 50 mM $ZnCl_2$, 450 mM NaCl was added; for 100 mM $ZnCl_2$, 300 mM NaCl; and for 200 mM $ZnCl_2$, no additional NaCl was required. The pH was adjusted to 1 or 3 by adding 32 % HCl (Th. Geyer GmbH, Renningen, Germany). The final amount of distilled water was adjusted to achieve a total protein concentration of 15 g per 100 g solution, considering both the volume of acid added and the moisture content of the WPI (dry matter content was measured using a moisture analyser (Kern & Sohn GmbH, Balingen, Germany) to be 93.09 ± 0.04 %, n = 3). Calcium-loaded WPI solutions were prepared analogously using $CaCl_2$ (≥99 %, p.a., Merck KGaA, Darmstadt, Germany) instead of $ZnCl_2$. Additionally, control samples containing only NaCl at a concentration of 600 mM were prepared. All experiments were conducted in triplicate. After adjusting the final composition, the solutions were sonicated for 15 min in an ultrasonic bath to ensure full hydration of the whey proteins. For gelation, 30 g of each sol was transferred into polypropylene screw-cap containers and sealed. The samples were then placed in an oven preheated to 80 °C for 2 h to induce gelation. After gelation, the resulting hydrogels were cooled to room temperature.

To enable supercritical drying, the water within the hydrogel pores was exchanged with ethanol. Hydrogels were treated twice with 150 g ethanol (≥99,8 v%, Carl Roth GmbH & Co. KG, Karlsruhe, Germany), added directly into the polypropylene containers. The two-phase system (hydrogel/ethanol) was gently agitated with a spatula to enhance solvent exchange efficiency. Following the initial ethanol addition, samples were left overnight at 22 °C. The ethanol content in the supernatant was determined by withdrawing a small aliquot with a polypropylene syringe and analysing it with a densitometer. To prevent particulate contamination, a PTFE syringe filter was used. After the ethanol content exceeded 90 w%, the supernatant was decanted, and a second exchange with fresh ethanol was performed. When the ethanol content in the supernatant exceeded 98 w%, samples were transferred into parcels from filter paper, sealed, and stored in ethanol until supercritical drying. During each stage (sol, hydrogel, and alcogel), aliquots were taken and dried at 60 °C for two days. These samples were analyzed for metal content to monitor potential metal ion losses during processing.

Finally, alcogels were dried in a custom-made 250 mL-autoclave using supercritical CO_2. Two samples in sealed filter paper parcels were placed into the preheated autoclave at 40 °C. The pressure was then slowly increased to above 100 bar by opening the CO_2 valve, starting supercritical drying. CO_2 and extracted ethanol were continuously vented from the reactor. After 4 h, the process was terminated by depressurizing the chamber at a rate of 5 bar/min to atmospheric pressure.

2.2. Liquid-chromatography mass spectrometry (LC-MS)

The amount of β-LG in the samples was quantified with LC-MS/MS using a bottom-up approach, based on the multiple reaction monitoring (MRM) analysis of specific marker peptides after tryptic hydrolysis (von Oesen et al., 2023). Briefly, proteins were extracted in an aqueous solution of 60 mmol/L tetrabutylammonium bromide (TEAB, Merck KGaA, Darmstadt, Germany) and 6 mol/L urea (Sigma-Aldrich, St. Louis, USA) under sonification, followed by reduction with a final concentration of 22 mmol/L tris(2-carboxyethyl)phosphine (TCEP, Alfa Aesar GmbH, Karlsruhe, Germany) for 20 min at 50 °C and alkylation with a final concentration of 16 mmol/L iodacetamid (IAA, Merck KGaA, Darmstadt, Germany) for 30 min at 50 °C in the dark. Samples were digested with a total amount of 0.2 mg trypsin (bovine pancreas, 10,000 BAEE units/mg protein, Sigma-Aldrich, St. Louis, USA) for 15 min at 50 °C and 50 W, using a microwave synthesizer CEM Discover SP (CEM GmbH, Kamp-Lintfort, Germany). After the addition of 100 μL 2 M acetic acid, undigested proteins were precipitated with ice-cold acetonitrile (Carl Roth GmbH & Co. KG, Karlsruhe, Germany) at −20 °C for 10 min followed by a centrifugation step (10,000×*g* at 4 °C). Subsequently, peptides in the supernatant were diluted in an aqueous solution of 2 % acetonitrile and 0.1 formic acid and quantified with LC-MS/MS on an Agilent G6470A Series Triple Quad LC/MS system (Agilent Technologies Deutschland GmbH, Waldbronn, Germany) measuring the product ions in Table 1 and using an external calibration with the reference peptide GLDIQK.

For chromatographic separation, a Waters XSelect HSS T3 LC column (3.5 μm, 150 × 2.1 mm) (Waters Corporation, Milford, MA, USA) was used at a flow rate of 0.4 mL/min, a column temperature of 40 °C and a binary solvent gradient, consisting of acetonitrile with 1 % formic acid (solvent A) and 0.1 % formic acid in water (solvent B). The following solvent gradient was applied: 0 min–2 % A, 0–3 min; 2 % A, 3–5 min; 2–6 % A, 5–10 min, 6–25 % A; 10–11 min, 25–50 %; 11–14 min, 50–90 %; 14–15 min, 90–2 % A, 15–20 min, 2 % A. MS analysis was performed in the positive ion mode using electrospray ionization (ESI) with a capillary current of 4200 nA and sheath gas (N_2) temperature of 300 °C. Collision energy for fragmentation of the product ions was according to von Oesen et al. (2023) and individually optimized when necessary (Table 1).

Table 1
Marker peptides used for LC-MS/MS analysis (CE = collision energy).

Protein	Analyte	Precursor ion $[(M+2H)^{2+}]$	Product ions		Product ions	
			$[(M+H)+]$ (m/z)	CE (eV)	$[(M+H)+]$ (m/z)	CE (eV)
β-LG	GLDIQK	337.2	503.2	8	388.2	8
		337.2	275.2	8	171.0	8

2.3. Flame atomic absorption spectrometry

A FAA spectrometer (PerkinElmer Analyst 800, PerkinElmer GmbH, Rodgau, Germany) was used to quantify the calcium and zinc content in protein samples at different steps of aerogel processing. Precisely weighed amounts of powders from the initial protein solution, hydrogel, alcogel, and aerogel samples were subjected to microwave-assisted digestion (Mars 6, CEM GmbH, Kamp-Lintfort, Germany) with a 1:1 mixture of ultrapure HNO_3 (65 %) and H_2O_2 (30 %) containing 15 mg/L magnesium as an internal standard to account for possible liquid losses during microwave digestion. Recovery efficiencies between 85 % and 95 % were incorporated into the metal quantification process using appropriate correction factors. For each of the metals limit of detection (LOD) and limit of quantitation (LOQ) were determined according to DIN 32645 ($n = 10$, $p < 0.05$). Analytical parameters were LOD 0.002 mg/L; LOQ 0.003 mg/L for magnesium; LOD 0.08 g/l; LOQ 0.26 mg/L for calcium and LOD 0.02 mg/L; LOQ 0.06 mg/L for zinc.

2.4. Fourier-transform-infrared spectroscopy (FTIR)

FTIR spectra of WPI and aerogels were recorded using a Tensor II infrared spectrometer (Bruker Optik GmbH, Karlsruhe, Germany) equipped with a Platinum attenuated total reflection (ATR) measurement cell and a nitrogen-cooled detector. The spectra were acquired in the wavenumber range of 3000–1000 cm^{-1} with a resolution of 2 cm^{-1} and each measurement consisted of 120 scans. To minimize deviations caused by uneven sample application, each sample was measured three to five times. The ATR cell was cleaned with ethanol between different sample measurements and background correction was performed against air. With the software OPUS 7.5, the recorded absorption spectra were subjected to offset correction in the wavenumber range of 1810–1800 cm^{-1}. The second derivative of the spectra was calculated by first performing vector normalization (1715–1475 cm^{-1}), followed by second derivative computation using the Savitzky-Golay algorithm with 25 smoothing points.

2.5. Brunauer-Emmett-Teller (BET) analysis

The specific surface area of the aerogels was determined via nitrogen adsorption-desorption measurements. For this purpose, 20–30 mg of each sample was weighed into a sample holder and degassed under vacuum at 60 °C for several hours to remove adsorbed moisture and gases. After degassing, the sample was re-weighted and the measurements were performed using a BET surface area analyser (Nova 3000e Surface Area Analyzer, Anton Paar QuantaTec Inc. Boynton Beach, FL, USA). The BET method was used in the p/p_0 range of 0.027–0.27 to estimate the mass specific surface area.

2.6. Scanning electron microscopy (SEM)

Microstructural imaging of the aerogels was conducted using a Supra VP55 scanning electron microscope (Carl Zeiss AG, Oberkochen, Germany). Prior to imaging, all samples were sputter-coated (Sputter Coater SCD 050, BAL-TEC, Balzers, Liechtenstein) with a thin layer of gold (~6 nm) to ensure conductivity. SEM images were captured at an accelerating voltage of 4 kV and a working distance ranging from 5.8 to 7.7 mm using an in-lens detector.

2.7. Sodium dodecyl sulfate-polyacrylamide gel electrophoresis (SDS-PAGE) of tryptic digested aerogels

2.7.1. Tryptic digestion

A trypsin solution was prepared by dissolving 50 mg of trypsin (1:250, min. 250 USP U/mg, porcine pancreas, AppliChem GmbH, Darmstadt, Germany) in 50 mL of phosphate buffer (pH 7.5). Approx. 35 mg of aerogel sample was incubated with 1500 μL of the trypsin solution at 37 °C in a heated shaker (AccuTherm, Faust Lab Science GmbH, Klettgau, Germany) at 650 rpm for 6 h. The amounts of zinc-loaded aerogels were adjusted to reach a final concentration of 5 mM zinc in the trypsin digest solutions. As controls, either WPI or phosphate buffer (pH 7.5) without aerogel was used under the same conditions. To terminate the digestion process, all samples were stored at -80 °C until further analysis.

2.7.2. SDS-PAGE

Digested aerogel and control samples were diluted 1:5 with phosphate buffer (pH 7.5) and subsequently mixed 1:1 with sample buffer, consisting of 25 μL 2-mercaptoethanol (≥99 %, Merck KGaA, Darmstadt, Germany), 250 μL Laemmli sample buffer (4 × concentrated, Bio-Rad Laboratories GmbH, Feldkirchen, Germany), and 750 μL bidistilled water. The samples were then incubated at 95 °C for 5 min to ensure protein denaturation. The electrophoresis chamber was filled with running buffer, which was prepared by diluting tris-glycine buffer (10 × concentrated, Hercules, Bio-Rad Laboratories GmbH, Feldkirchen, Germany) 1:10 with bidistilled water. Following incubation, 5 μL of protein standard and 20 μL of each sample were loaded into the wells of polyacrylamide gradient gels (4–20 %, Mini-PROTEAN® TGX Stain-Free™, Bio-Rad Laboratories GmbH, Feldkirchen, Germany). The gels were assembled in the electrode chamber of the electrophoresis system (Mini-PROTEAN® Tetra, Bio-Rad Laboratories GmbH, Feldkirchen, Germany), and electrophoresis was performed at a constant voltage of 100 V. Upon completion, the gels were removed from the chamber and transferred to the tray of a GelDoc Go Imaging System (Bio-Rad Laboratories GmbH, Feldkirchen, Germany) for visualization. Imaging was performed under UV-light using the provided Image Lab 6.1 software with an exposure time of 2 × 45 s.

2.8. Cell experiments

Caco-2 cells were obtained from the European Collection of Authenticated Cell Cultures (ECACC, Porton Down, UK). Cells were regular cultivated in DMEMphenol red (PAN-Biotech GmbH, Aidenbach, Germany) containing 10 % fetal calf serum (FCS) (c.c.pro GmbH, Oberdorla, Germany), 100 U/mL penicillin and 100 μg/mL streptomycin (PenStrep, Sigma-Aldrich, St. Louis, USA) at 37 °C in a humidified 5 % CO_2 atmosphere. For zinc uptake studies, Caco-2 cells were plated in 96-well plates (5000 cells per well) and cultured for 21 d to develop into an enterocyte-like monolayer, accordingly (Maares et al., 2018a). Cellular zinc uptake was analyzed using the fluorescent probe Zinpyr-1 according to Burdette et al. (2001), following the protocol described by Maares et al. (2018b). After 30 min of treatment with 2.5 μM Zinpyr-1 in incubation buffer (120 mM NaCl, 5.4 mM KCl, 5 mM glucose, 1 mM $CaCl_2$, 1 mM $MgCl_2$, 1 mM NaH_2PO_4, 10 mM HEPES, 0.3 % BSA, pH 7.35), supernatants were removed and the adherent cell monolayers were washed twice with assay buffer (incubation buffer w/o BSA) to remove extracellular Zinpyr-1. Next, cells were treated with 100 μL of either assay buffer (control cells) or buffer containing 10 μM of $ZnCl_2$ or $ZnSO_4$. A concentration of 10 mg WPI/mL was employed for co-incubation with 10 μM $ZnSO_4$. The aerogel digestion solutions were diluted 1:500 in assay buffer before cell application. Zinpyr-1 fluorescence ($\lambda ex = 492$ nm and $\lambda em = 527$ nm) was measured after 120 mincell treatment using a fluorescence plate reader (Tecan Infinite M200; Tecan Austria GmbH, Grödig/Salzburg, Austria).

2.9. Statistical evaluation

All experiments were performed in independent triplicate. Normality was tested using the Kolmogorov-Smirnov test, and homogeneity of variance was assessed with Levene's test. Each dataset was analyzed using a *one-way* or *two-way* ANOVA, considering the type of metal and the pH of the initial solution as factors, followed by Tukey's test to identify significant differences ($p \leq 0.05$). All statistical analyses were

performed using GraphPad Prism 8 (GraphPad Software Inc., Boston, USA).

3. Results and discussion

This study provides a comprehensive analysis of zinc incorporation into WPI-based aerogels, including their chemical composition, structural and morphological properties, proteolytic digestibility, and zinc bioavailability in a Caco-2 intestinal cell model.

3.1. β-lactoglobulin content and ion retention along aerogel preparation process

The protein composition of the WPI-based aerogels was analyzed at each stage of preparation, including the initial solution, the hydrogel, the alcogel, and the final aerogel. As expected, β-LG was the predominant protein component of starting WPI, constituting approx. 50 % of the total protein (relative to dry matter), while in solution its relative content was lower (approx. 20–40 %), likely reflecting its initial distribution at this stage (Fig. 1).

At pH 1, β-LG contents increased progressively across all treatment steps – from solution through hydrogel and alcogel to the final aerogel – ultimately reaching the highest concentrations in the aerogel for all samples, although not all increases were statistically significant. This upward trend confirms the stepwise concentration of β-LG during gelation, solvent exchange and drying, likely driven by its strong self-association and preferential retention within the forming network. Although the composition of other proteins was not systematically determined, α-lactalbumin levels remained largely constant (data not shown), indicating that the observed increase in β-LG cannot be explained solely by a decrease of other proteins. Another explanation for the stepwise increasing β-LG amount may be a reduced proteolytic susceptibility due to the gel formation. However, the peptide used for quantification (GLDIQK) is located near the N-terminus of the primary protein sequence – an area easily cleaved by trypsin even in native protein (Fernández & Riera, 2013). Thus, diminished tryptic digestibility appears to be neglectable. Intriguingly, the β-LG content in zinc-containing solutions was consistently lower than in those with calcium or sodium, although, again, not all differences reached statistical significance. This trend may reflect the more localized or weaker coordination interactions of zinc ions with specific residues in β-LG, in contrast to the broader crosslinking potential of calcium ions, which may facilitate more efficient protein-protein interactions in the early gelation process. As a result, early β-LG interactions with zinc may be less extensive, leading to lower apparent concentrations before solvent removal. The subsequently steeper increase in β-LG content during aerogel formation in zinc-containing systems likely reflect the structural sensitivity of Zn^{2+}-coordinated networks during solvent removal, which can promote local enrichment of β-LG as the network further contracts. Despite these initial differences, all systems converged to similarly high β-LG contents in the aerogel stage, suggesting that solvent removal and network formation network consistently retained the protein.

At pH 3, β-LG contents remained comparatively consistent across all systems, indicating that the metal ion type had less influence than at pH 1. This 'stability' likely arises from β-LG's lower net charge near its isoelectric point of 5.4 (Sawyer & Kontopidis, 2000), thereby, reducing electrostatic repulsion and promoting self-association. The most substantial concentration of β-LG again occurred between the transition from alcogel to aerogel, underscoring the critical role of solvent removal. The higher variability observed in zinc-containing aerogels may reflect structural sensitivities in Zn^{2+}-coordinated networks during the drying process.

Regarding the chemical composition of aerogels, the retention of calcium and zinc in WPI and respective aerogels was analyzed in dependence of the initial metal ion concentration and the preparation stages using FAAS (Fig. 2). The calcium content of WPI was 1.62 ± 0.04 mg/g, whereas the zinc content was below the LOQ of the FAAS method, indicating only trace amounts of zinc in WPI (data not shown). Moreover, aerogels prepared with NaCl retained calcium levels similar to native WPI, and zinc remained below the quantification limit, indicating that the inherent metal ion content was preserved and no contamination occurred during the aerogel preparation process (data not shown). The analysis of aerogels revealed that the final metal ion content increased with the concentration of $CaCl_2$ or $ZnCl_2$ in the initial solution (Fig. 2A and B). As expected, the highest metal ion concentrations were found in aerogels derived from solutions with 200 mM $CaCl_2$ or $ZnCl_2$. Calcium-containing aerogels obtained from the more acidic solutions, exhibited a calcium content of 8.0 ± 2.0 mg/g, corresponding to a retention percentage of 17.9 %. Similarly, the zinc content in aerogels at pH 1 was 13.0 ± 1.0 mg/g, with 19.0 % of the initially incorporated zinc retained. These results indicate that metal ion binding under strongly acidic conditions in the initial solution is limited, likely due to the extensive protonation of binding sites, which reduces their ability to interact with metal ions.

Metal ion retention in aerogels prepared from 'pH 3 solutions', was significantly higher than at pH 1. Calcium-containing aerogels amounted 10.6 ± 0.7 mg/g of calcium, corresponding to a retention percentage of 23.7 %, while the zinc content reached 23.0 ± 0.4 mg/g, with a retention rate of 31.2 %. On average, aerogels from solutions prepared at pH 3 exhibited 2.1-fold higher calcium and 1.6-fold higher zinc contents than those with pH 1, despite identical metal ion concentrations in the initial solutions. This pH-dependence might be explained by the

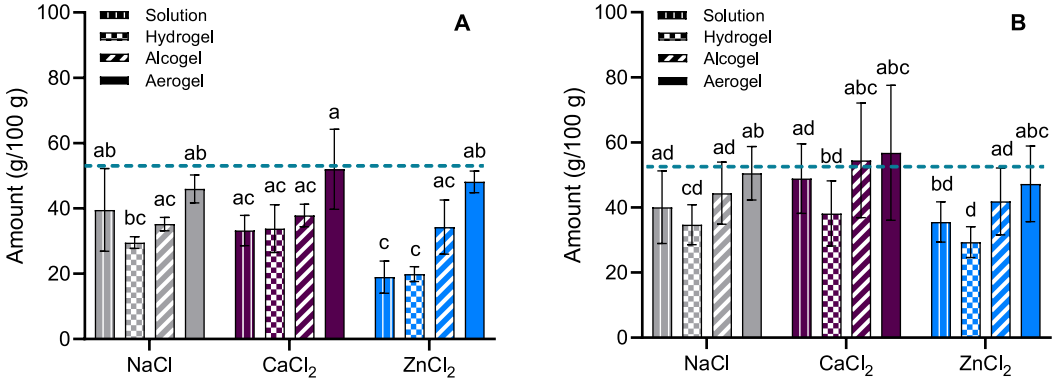

Fig. 1. Liquid chromatography-mass spectrometry analysis of β-lactoglobulin content relative to dry matter in whey protein isolate (dotted line, significance level a) and its dependence on the aerogel preparation process, including solution, hydrogel, alcogel, and aerogel containing 600 mM NaCl, 200 mM $CaCl_2$, or 200 mM $ZnCl_2$. (A) Data at pH 1. (B) Data at pH 3. Means that differ with statistical significance do not share the same letters and error bars represent standard deviation ($p < 0.05$, *two-way* ANOVA).

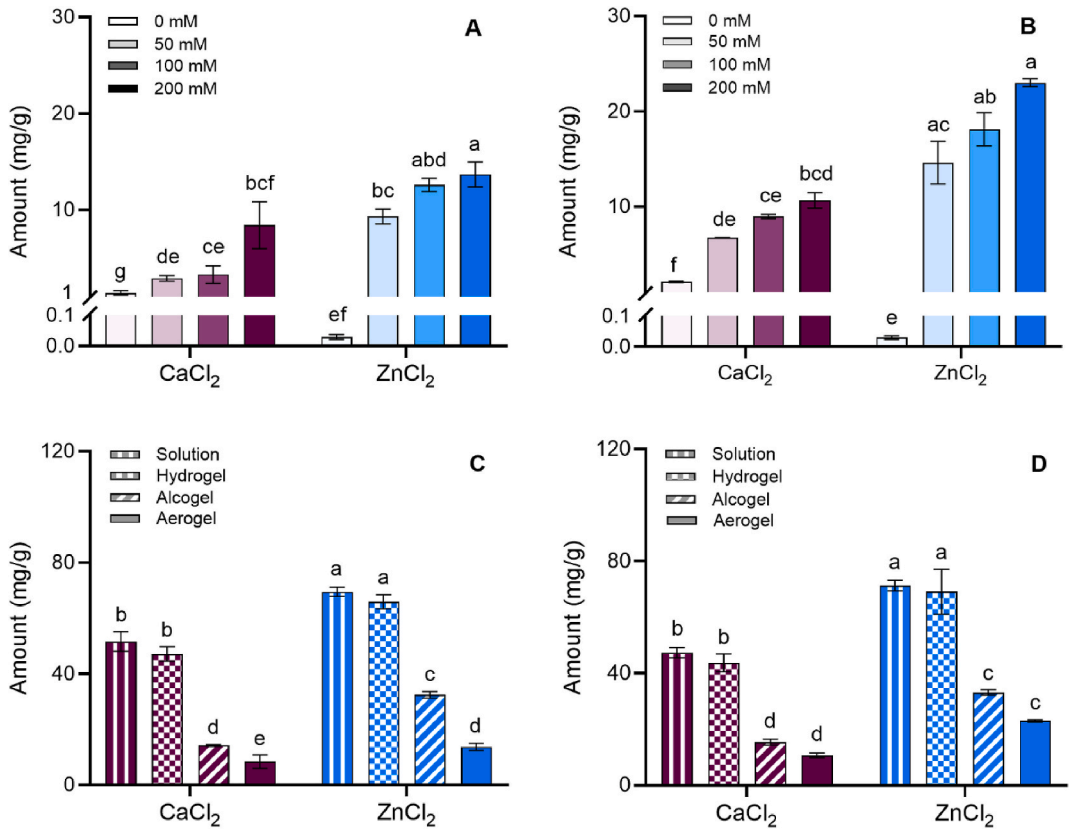

Fig. 2. Flame atomic absorption spectrometry determination of Ca and Zn throughout WPI aerogel preparation steps, relative to the dry matter. Amounts of Ca and Zn in the aerogel samples in dependence on the initially added salt concentration (0, 50, 100, or 200 mM) for (A) pH 1 and (B) pH 3 and in dependence on the preparation step (solution, hydrogel, alcogel, and aerogel) for (C) pH 1 and (D) pH 3 for samples prepared with an initial salt concentration of 200 mM. Means that differ with statistical significance do not share the same letters and error bars represent standard deviation ($p < 0.05$, *two-way* ANOVA).

interaction mechanisms of metal ions with proteins, which occur through specific amino acid binding sites. For instance, in α-LA, calcium binds strongly at a well-defined site composed of amino acids lys79, asp82, asp84, asp87, and asp88, while zinc can also bind at this region, but additionally interacts with aspartic acid, glutamate, histidine and cysteine (Buszewski et al., 2020; Rodzik et al., 2020). In fact, metal ion binding in proteins is highly influenced by amino acid residues with charged side chains (such as aspartate, glutamate, and histidine) which provide coordination sites through electrostatic and coordinate interactions. In the main component β-LG, at pH 3, some acidic residues like those of aspartate and glutamate are near their pKa and thus, partially deprotonated (Kleemann et al., 2020), while histidine residues may also participate, potentially enabling limited interactions with divalent metal ions. At pH 1, extensive protonation results, however, in a predominantly positive charge, weakening the metal ion interactions, and leading to the hypothesized lower metal retention as compared to pH 3. Kallay et al. (2005) demonstrated a similar effect in Cu^{2+}-oligopeptide complexes, where deprotonated peptides bound copper more effectively than protonated peptides, thereby stabilizing the Cu^{2+}-peptide species. Similarly, Udechukwu et al. (2018) found that whey-derived peptides with negatively charged amino acid residues bind zinc efficiently and correlated the subsequent zinc retention with the charge of the peptides. These studies collectively indicate that metal ion retention depends on pH and, consequently, on the charge of the proteins, aligning with the observed pH-dependent differences in metal retention in aerogels in the present study.

Regarding the aerogel preparation process, calcium and zinc concentrations of 200 mM remained stable between the initial solutions and the hydrogels (Fig. 2C and D). However, the hydrogel-to-alcogel transition resulted in substantial calcium losses of 70 % at pH 1 and 65 % at pH 3, while zinc decreased by only approx. 50 % at both pH values. These significant ion losses are most likely driven by solvent removal, which shifts the equilibrium between protein-bound and free dissolved ions. As reported in literature, calcium and zinc ions are more soluble in water than in ethanol (Cao et al., 2001; Gomis et al., 2013; Hao et al., 2023), a property that facilitate their extraction during solvent exchange. In fact, the gradual replacement of water by ethanol weakens protein-ion interactions, allowing ions to redistribute into the bulk solvent phase even though their absolute solubility in ethanol is lower than in water. Beyond solubility effects, the transition to an ethanol-rich environment also alters protein interactions, thereby influencing the structural and network properties of the gel and ultimately affecting metal retention. The replacement of water with ethanol disrupts the protein's hydration shell, leading to structural rearrangements (Kleemann et al., 2020). As ethanol is a weaker hydrogen bond donor than water, it destabilizes intramolecular hydrogen bonds, causing partial unfolding and conformational changes that may alter the availability of metal-binding sites such as aspartate and glutamate. Thus, the structural rearrangements may decrease accessibility of coordination amino acid side chains and weaken protein-ion interactions, allowing metal ions to redistribute into the bulk solvent phase and facilitating their release during solvent exchange. Additionally, at approx. 60 % ethanol, hydrophobic interactions and hydrogen bonding begin to counterbalance repulsive electrostatic forces, leading to a more compact gel network (Kleemann et al., 2020). At this stage, whey protein hydrogels typically undergo shrinkage, suggesting a denser packing of protein molecules in the alcogel compared to the hydrogels, which can reduce the hydration shell and weaken protein-ion interactions, thereby facilitating the substantial loss of metal ions observed in the present study. In addition, the ‚openness' and porosity of the protein network –

as discussed in Section 3.3 – may further facilitate ion diffusion and thus contribute to the pronounced losses observed under these conditions. During supercritical drying, calcium content decreased by 31 % at pH 3 but remained unchanged at pH 1, whereas zinc losses from the alcogels amounted to 58 % at pH 1 and 31 % at pH 3 (Fig. 2C and D). The overall higher retention of calcium and zinc at pH 3 compared to pH 1 suggests enhanced ion stabilization through stronger protein-metal interactions, particularly in the final processing step. This trend aligned with the proposed mechanism described before, indicating that metal ions in alcogels formed at pH 3 are retained more effectively than those from pH 1 due to the increased stabilization provided by charge effects.

3.2. Secondary structure analysis of aerogels

The secondary structure of WPI and aerogels with 600 mM NaCl, 200 mM $CaCl_2$ and 200 mM $ZnCl_2$ was analyzed using FTIR (Fig. 3). The FTIR spectrum of WPI exhibited the characteristic amide I and amide II bands of proteins, with maxima at 1630 cm^{-1} and at 1520 cm^{-1}, respectively (Fang & Dalgleish, 1997). Compared to WPI, the amide I band of aerogels prepared at pH 1 was broader, and the maximum shifted slightly to 1625 cm^{-1} (Fig. 3A). A similar shift was also observed in aerogels prepared at pH 3 (Fig. 3B), indicating alterations in the protein secondary structure of WPI during aerogel formation, as suggested by Plazzotta et al. (2020). These structural changes were further analyzed using the second derivative, which identified a distinct band at approx. 1635–1620 cm^{-1}, characteristic of intramolecular β-sheet structures (Fig. 3C and D). In aerogels prepared from solutions at pH 1, the intramolecular β-sheet band intensity was significantly higher containing calcium and zinc compared to WPI or aerogels containing sodium (Table 2). This trend may be linked to the β-LG content observed via LC-MS (Fig. 1), as β-LG's secondary structure consists mainly of intramolecular β-sheets (Tolkach & Kulozik, 2007). In particular, a higher β-LG content corresponds to an increased proportion of intramolecular β-sheets in the aerogels. Moreover, the significant shift of the intramolecular β-sheet band towards lower wavenumbers (Table 2) suggests a reduction in the electron density at the carbonyl group,

Table 2
Fourier-transform-infrared spectroscopy analysis of wavenumber and intensity of the intramolecular β-sheet band of whey protein isolate and whey protein isolate-based aerogels containing 600 mM NaCl, 200 mM $CaCl_2$, or 200 mM $ZnCl_2$ at approx. 1630 cm^{-1}. Different letters indicate statistically significant differences (*two-way* ANOVA, $p \leq 0.05$).

	pH 1		pH 3	
Aerogel	Wavenumber	Intensity	Wavenumber	Intensity
WPI	1628.1 ± 0.1[a]	−0.00052 ± 0.00002[a]	1628.1 ± 0.1[a]	−0.00052 ± 0.00002[a]
600 mM NaCl	1625.6 ± 0.2[b]	−0.00040 ± 0.00014[a]	1624.0 ± 0.2[b]	−0,00079 ± 0.00016[b]
200 mM $CaCl_2$	1623.4 ± 1.0[c]	−0.00070 ± 0.00003[b]	1625.5 ± 0.5[c]	−0,00070 ± 0.00003[b]
200 mM $ZnCl_2$	1623.4 ± 0.1[c]	−0.00081 ± 0.00003[b]	1623.5 ± 0.1[b]	−0,00048 ± 0.00002[a]

indicating the formation of additional or stronger hydrogen bonds within the aerogel structures compared to WPI, accordingly (Jackson & Mantsch, 1995). This red shift of the wavenumbers is consistent with earlier observations for purified β-LG in the presence of NaCl at neutral pH compared to β-LG without added salt (Kieserling et al., 2021), indicating that both salt effects and the solvent-induced gelation process contribute to the altered secondary structure in the aerogels. As reviewed by Betz et al. (2012), similar intermolecular interactions are proposed to occur in both hydrogels and aerogels. The present findings confirm that hydrogen bonds, in particular, play a crucial role in the structural stability of aerogels, supporting the idea that the balance of non-covalent interactions shifts during the aerogel preparation process, favoring hydrogen bonds in the final structure. This observation is further supported by Ahmadi et al. (2016), who demonstrated by FTIR analysis that whey protein-based aerogels exhibited strong hydrogen bonding.

The effect of metal ions on the secondary structure of whey protein aerogels was also evident in the pronounced shift of the intramolecular β-sheet band towards lower wavenumbers, which was more significant

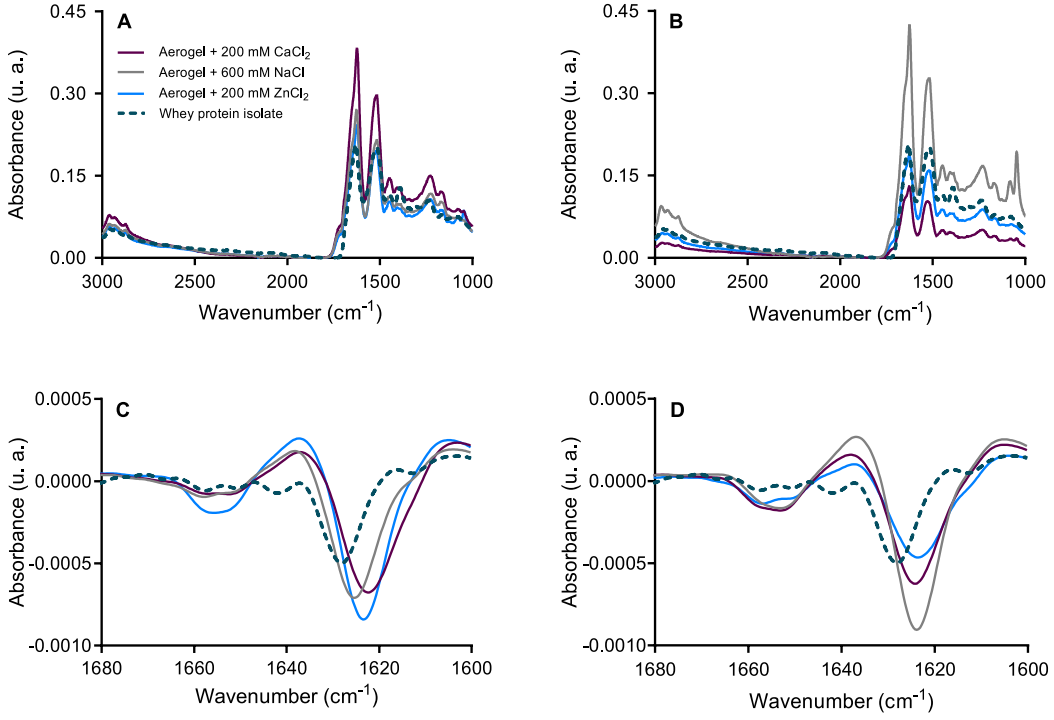

Fig. 3. Fourier-transform-infrared spectroscopy of whey protein isolate and whey protein isolate-based aerogels containing 600 mM NaCl, 200 mM $CaCl_2$, or 200 mM $ZnCl_2$. Off-set corrected spectra (A) at pH 1 and (B) at pH 3, and second derivative spectra of the amide I band (A) at pH 1 and (B) at pH 3.

in aerogels containing calcium and zinc than in those containing sodium (Table 1). This shift suggests stronger interactions between divalent metal ions (Ca^{2+} and Zn^{2+}) and the protein matrix than with monovalent ions like Na^{+}, with potential involvement of the carbonyl groups of peptide bonds in metal coordination. These findings align with studies described by Wang et al. (2023) and Liu et al. (2019), which demonstrated distinct zinc binding to casein or sea cucumber peptides via their carbonyl groups using FTIR analysis, respectively. Divalent metal ions might not only exhibit stronger interactions with the protein than monovalent ions, due to their higher charge density, which enhances electrostatic attraction to charged amino acid residues, but they may also directly coordinate with the carbonyl groups of the protein backbone. In fact, Wang et al. (2024) reported a similar wavenumber shift in the FTIR spectra for WPI-based aerogels containing calcium ions and furthermore highlighted the role of hydrophobic and electrostatic interactions in stabilizing these aerogel systems. In contrast to divalent ions, monovalent sodium ions have a lower charge density, leading to less pronounced structural modifications in the aerogel network. Hence, the combination of metal coordination, charge effects, and alterations in protein-protein interactions suggests that divalent ions contribute to network stabilization and modulate hydrogen bonding.

Adjacent to the β-sheet band, the random coil band at approx. 1640 cm^{-1} appeared more pronounced in the aerogel spectra compared to WPI, suggesting partial unfolding of the protein structure during aerogel formation. This structural alteration was expected under the applied gelation conditions for the hydrogel (heating at 80 °C for 2 h) and aligned with previous findings described in the literature (Lefevre & Subirade, 1999; Nicolai et al., 2011). Regarding the influence of metal ions, no significant shifts in the random coil wavenumber were observed. However, zinc ions seem to induce slightly more partial unfolding than calcium and sodium ions. This effect may be attributed to the stronger coordination ability of zinc, which can interact with various amino acid residues compared to other divalent ions as calcium (cf. Section 3.1), thereby destabilizing the initial protein structure. Additionally, zinc is known to influence protein hydration shells by competing with water molecules for binding sites, as recently demonstrated by Yue et al. (2022) for collagen molecules. This competition further contributes to conformational changes in the protein structure.

Moreover, intermolecular β-sheets are more prominent in aerogels than in WPI, suggesting the formation of β-sheet structures during the aerogel preparation process (Fig. 3). As Kieserling et al. (2021) showed for pure β-LG at neutral pH, NaCl slightly reduces intermolecular β-sheets, indicating that in the present study the enhanced signals may arise primarily from structural rearrangements during aerogel formation rather than from salt addition. While hydrophobic interactions between protein strands contribute to gelation in hydrogels (Mezzenga & Fischer, 2013), the pronounced intermolecular β-sheet band suggests that β-sheet aggregation – and possibly the formation of partially aligned β-sheet aggregation (Hoppenreijs et al., 2023) – also plays a crucial role in stabilizing the aerogel network. A comparable finding was reported by Plazzotta et al. (2020), who compared the FTIR spectra of WPI and whey protein-based aerogels and observed an increase in intermolecular β-sheet content in the aerogel. Furthermore, all metal ions shift the intermolecular β-sheet band towards lower wavenumbers, indicating, similarly to the intramolecular β-sheets, an increase in the number and strength of hydrogen bonds within intermolecular aggregates (Jackson & Mantsch, 1995). This effect can be explained by the ability of metal ions to bridge adjacent protein molecules, facilitating closer packing and promoting hydrogen bond formation. Divalent ions, such as Ca^{2+} and Zn^{2+}, are particularly effective in this process due to their high charge density, which enhances electrostatic interactions and stabilizes β-sheet-rich protein assemblies. By contrast, monovalent ions like Na^{+} exert a weaker influence, as their lower charge density results in less pronounced structural rearrangements within the aerogel network.

In aerogels prepared from solutions at pH 3, the FTIR second derivative spectra exhibited structural changes similar to those observed in aerogels obtained from solutions at pH 1 (Fig. 3D), particularly in terms of random coil content and intermolecular β-sheet formation. The intensities of the intramolecular β-sheet bands also remained relatively stable compared to pH 1, except for aerogels containing NaCl, which showed the highest amount of intramolecular β-sheets. As discussed above, this trend is likely associated with a high β-lactoglobulin content (Fig. 2), which promotes β-sheet formation. Moreover, the shift of the intramolecular β-sheet band towards lower wavenumbers persisted at pH 3, indicating an increased number or strength of hydrogen bonds in aerogels compared to WPI (Jackson & Mantsch, 1995). This suggests that the structural reorganization and stabilization mechanisms during aerogel formation at pH 1 and pH 3 are largely similar. However, some degree of pH dependence is still expected, as the lower protonation state at pH 3 compared to pH 1 may influence interactions with metal ions (cf. Section 3.1). At pH 3 in particular, deprotonated carboxyl side chains of aspartate and glutamate are more available for metal ion binding, potentially reducing the involvement of carbonyl groups in coordination. This assumption is supported by findings described by Si et al. (2023), who demonstrated by FTIR and NMR analyses that Ca^{2+} ions preferentially bind to the carboxyl groups of asparagine and glutamic acid in phosphovitin peptides. Consequently, it can be considered that electrostatic interactions play a more prominent role in metal binding at pH 3, whereas at pH 1, alternative coordination sites, such as carbonyl groups, may contribute more. This shift in metal-binding mechanisms also affects the balance of non-covalent interactions, potentially influencing the overall network stability and mechanical properties of the aerogels.

3.3. Surface and morphological properties of aerogels

To characterize the surface properties of the aerogels, specific surface area measurements were performed using BET analysis (Table 3). In aerogels obtained from solutions at pH 1, BET analysis revealed significant differences in surface area depending on the added metal ions. While aerogels containing NaCl exhibited no measurable surface area, those prepared with $CaCl_2$ and $ZnCl_2$ showed values of 270 ± 70 m^2/g and 156 ± 136 m^2/g, respectively, suggesting that divalent ions promote structural modifications that enhance aerogel porosity (Table 3). The large standard deviation observed for $ZnCl_2$-loaded aerogels reflects the inherent heterogeneity and structural sensitivity of the material, indicating that variations in synthesis conditions can substantially influence porosity. These relatively high standard deviations should be considered when interpreting the BET-derived surface area results.

Compared to previously reported no-salt-added protein aerogels, which often exhibit very high specific surface areas (up to several hundred m^2/g) and pronounced mesoporosity (Andlinger et al., 2022; Jung et al., 2023; Plazzotta et al., 2021; Schroeter et al., 2021), the aerogels obtained in this study showed considerably lower surface areas and denser microstructures. This divergence can be explained by the different gelation conditions: in salt-free systems and low pH, rapid protein unfolding (induced by strong electrostatic repulsion) exposes hydrophobic groups, leading to short, rigid aggregates stabilized mainly by non-covalent interactions. This results in a dense but irregular aerogel network with high mesoporosity The additional presence of

Table 3
Brunauer-Emmett-Teller analysis of the surface area of aerogels containing 600 mM NaCl, 200 mM $CaCl_2$, or 200 mM $ZnCl_2$. Means that differ with statistical significance do not share the same letters (*two-way* ANOVA, $p \leq 0.05$).

	Surface area (m^2/g)	
Aerogel	pH 1	pH 3
600 mM NaCl	n. d.	32 ± 55^{a}
200 mM $CaCl_2$	270 ± 70^{b}	n. d.
200 mM $ZnCl_2$	156 ± 136^{b}	n. d.

n. d. = not detected.

divalent ions in our experiments promoted charge screening, localized coordination, and enhanced β-sheet formation, resulting in more compact networks. Thus, our findings complement the existing literature by highlighting how ion-specific interactions shift the aerogel structure away from the highly mesoporous morphology typically observed in no-salt-added protein aerogels.

Intriguingly, previous studies demonstrated that divalent calcium ions can act as crosslinkers in hydrogel and aerogel networks. For instance, Liang et al. (2020) described whey protein-based hydrogels containing calcium ions as 'cloud-like', forming large aggregates with highly porous structures compared to those without calcium. Those authors attributed these porous structures to the ions' ability to form bridges (i.e., electrostatic salt bridges) between anionic amino acid residues, such as deprotonated carboxyl groups (cf. Section 3.1). It should be emphasized that the effect of calcium on aerogel morphology strongly depends on the gelation environment. For instance, Liang et al. (2020) observed more open structures in calcium-containing hydrogels at near-neutral pH, while our systems were prepared under strongly acidic conditions. At low pH, carboxyl groups are largely protonated and therefore less available for ionic bridging. Under these conditions, calcium mainly contributes through charge screening and local coordination, which is consistent with the comparatively lower specific surface areas measured in our study (Table 3) and the formation of denser aerogel networks. By contrast, at higher pH values deprotonated carboxyl groups enable calcium to form bridges between protein chains: In this context, Mottola et al. (2025) suggested that calcium ions facilitate gelation in protein-based hydrogels through a mechanism similar to the "egg-box" model, which is commonly used to describe ionic crosslinking in polysaccharides. This model involves the coordination of divalent cations between polymer chains, thereby stabilizing the gel network. While it typically requires deprotonated carboxyl groups and is therefore less directly applicable under the acidic conditions used here, it nevertheless illustrates how calcium can act as a bridging ion. In the present study, such interactions may instead involve carbonyl oxygen, hydroxyl groups, or the limited fraction of residual carboxylates available at low pH. In Klicken oder tippen Sie hier, um Text einzugeben.the present study, however, a low proportion of negatively charged carboxyl groups, due to the high degree of protonation at low pH, was assumed to be present, suggesting that other functional groups or reaction partners, such as hydroxyl groups (e.g., serine, threonine, tyrosine) may be involved in the crosslinking process (cf. Sections 3.1 and 3.2). Liang et al. (2020) further reported a high water-holding capacity in calcium-containing gels, which was attributed to the formation of small pore sizes. In contrast, Niu et al. (2019) described near-neutral pH conditions and observed a reduced water-holding capacity in gelatin-alginate hydrogels upon calcium addition. Those authors explained this effect by the formation of a compact gel structure, as the presence of calcium ions reduced the electrostatic repulsion necessary for the development of porous networks. In relation to the transition from hydrogels to aerogels, FitzPatrick et al. (2022) showed that divalent calcium supports the retention of the gel network during solvent exchange in canola protein-based systems and helps to preserve the necessary porosity in the resulting aerogels. Overall, these findings indicate that the effects of divalent ions are protein-specific but also strongly influenced by environmental conditions such as pH. In the present study, the addition of divalent ions, in contrast to some earlier reports, resulted in the formation of a porous aerogel structure at pH 1. This highly 'open' network likely facilitated ion diffusion during solvent exchange and drying, which is consistent with the pronounced ion losses observed under these conditions (cf. Section 3.1).

However, BET analysis of aerogels obtained from solutions at pH 3, revealed a contrasting trend compared to pH 1. While aerogels prepared with NaCl exhibited a modest specific surface area with a high standard deviation (32 ± 55 m^2/g), no measurable surface area was detected for samples containing $CaCl_2$ and $ZnCl_2$. These results indicate the formation of dense, low-porosity structures in the presence of divalent ions at this pH. This observation can be explained by the proximity to the proteins' isoelectric point, where the reduction in electrostatic repulsion facilitates protein aggregation. Such aggregation favors the formation of compact, macroporous networks rather than open, mesoporous structures (Kleemann et al., 2018; Selmer et al., 2015). In contrast to the filamentous and highly porous networks observed at pH 1, where electrostatic repulsion is more pronounced and likely drives the formation of looser structures, the system at pH 3 appeared to shift toward extensive aggregation and structural collapse upon drying. The lack of measurable surface area in calcium- and zinc-containing samples suggests that, under these near-IEP conditions, divalent ions no longer enhanced porosity as they did at pH 1. Rather, their presence may promote tighter packing of protein aggregates, contributing to the formation of dense gels that do not retain a mesoporous structure during the aerogel transition. These findings further highlight the pH-dependent nature of ion-protein interactions for the final aerogel structure.

Morphological analysis using SEM (Fig. 4A–C, E) provided further insight into the structural differences induced by pH and ionic conditions during aerogel formation. SEM images of aerogels prepared from pH 1 solutions, revealed that whey proteins primarily formed large aggregates (with a characteristic size of hundreds of nanometers), contributing to a predominantly macroporous structure. However, finer, filamentous regions with smaller, mesoporous features were also visible – particularly in aerogels containing $CaCl_2$ and $ZnCl_2$ (see Fig. 4C–E, inset). These localized structures were consistent with the higher BET surface areas recorded for these samples and suggest that divalent cations may promote partial formation of more open, filament-like networks within an otherwise aggregated matrix (Table 3). Hence, as hypothesized, while acidic conditions promote aggregation due to reduced electrostatic repulsion, specific ion-protein interactions (i.e., particularly in the presence of divalent cations) can still influence network formation, leading to heterogeneous porosity.

In contrast, SEM images of aerogels prepared at pH 3 showed uniformly dense morphologies with large aggregate clusters and an absence of mesoporous or filamentous domains (Fig. 4B–D, F). This morphological compactness, reflected in the lower or absent BET surface areas, aligns with aggregation behavior near the proteins' isoelectric point. This interpretation is supported by Kharlamova et al. (2020), who showed that increased ionic strength enhances dense aggregation, and by Bryant & McClements (2000), who demonstrated that calcium concentration during gelation significantly affects whey protein hydrogel microstructure and rheologiy. The role of ionic strength becomes even clearer when comparing the present findings with those of Jung et al. (2023); despite using an identical pH in the sol solution, aerogels produced without additional ionic strength adjustments exhibited a finer, rather uniform morphology consisting of small, connected aggregates. This contrast suggests that the presence of divalent ions in the present study at pH 3 may have accelerated protein-protein interactions, thereby limiting the development of mesoporous networks and favoring dense, compact, macroporous structures instead. Together, these results emphasize the critical influence of both pH and ionic environment in governing the microstructural evolution of protein-based aerogels. Moreover, it should be noted that BET measurements primarily probe mesopores and micropores, and thus the lack of measurable surface area at pH 3 indicates the absence of significant mesoporosity. In contrast, SEM imaging reveals the presence of macroporous aggregates, highlighting that aerogels can still maintain a porous morphology at the microscale despite the absence of mesopores. Therefore, the apparently conflicting BET and SEM results are a consequence of the different length scales probed by these techniques.

3.4. Digestibility and zinc bioavailability of aerogels in Caco-2 cells

The SDS-PAGE analysis of the protein profiles of undigested and trypsin-digested WPI and aerogels containing 600 mM NaCl, 200 mM $CaCl_2$, or 200 mM $ZnCl_2$ are illustrated in Fig. 5. In the present study,

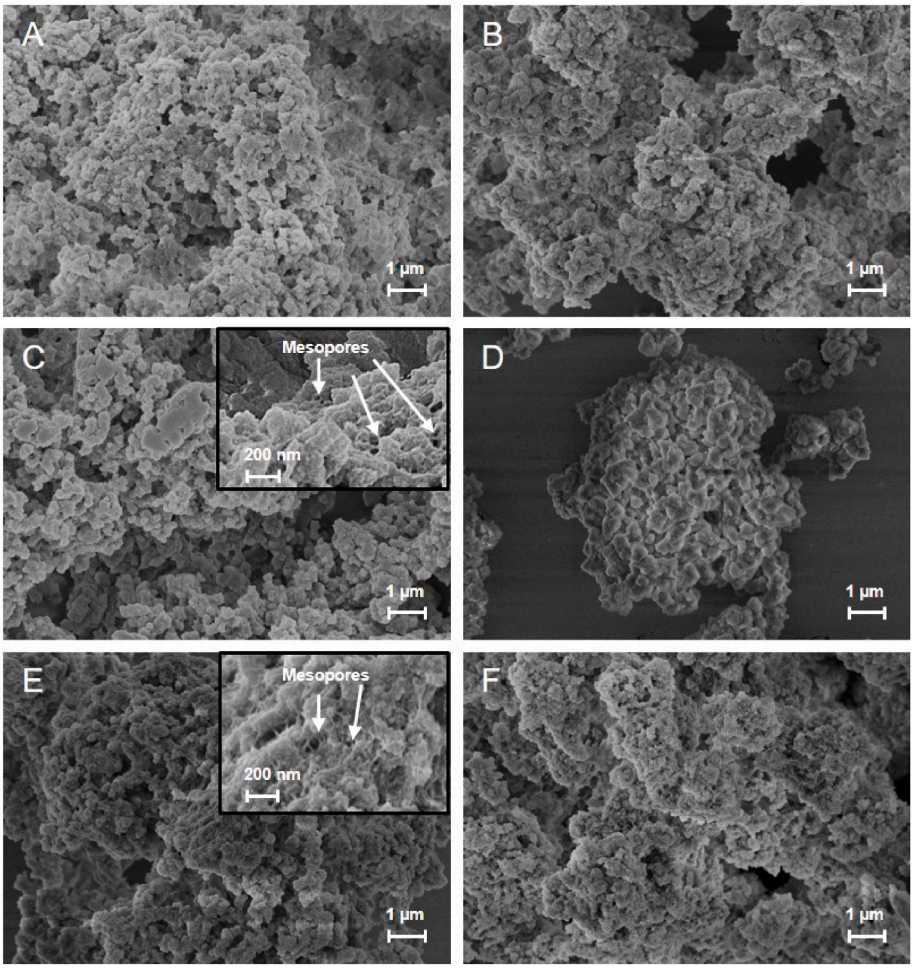

Fig. 4. Scanning electron microscope images of whey protein-based aerogels containing 600 mM NaCl (A) at pH 1, and (B) at pH 3; containing 200 mM $CaCl_2$ (C) at pH 1, and (D) at pH 3; or containing 200 mM $ZnCl_2$ (E) at pH 1, and (F) at pH 3.

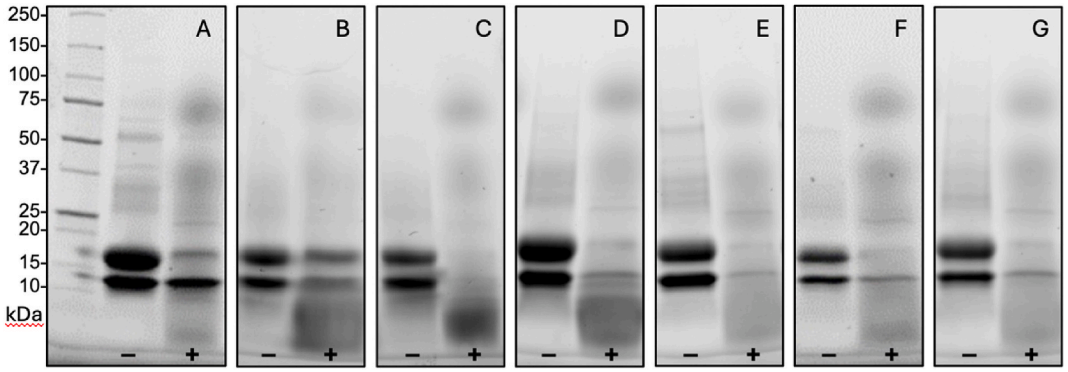

Fig. 5. Sodium dodecyl sulfate polyacrylamide gel electrophoresis (SDS-PAGE) analysis of samples without (−) and with (+) trypsin digestion. (A) Whey protein isolate, and whey protein-based aerogels, under different conditions; (B) 600 mM NaCl at pH 1, (C) 200 mM $CaCl_2$ at pH 1, (D) 200 mM ZnCl2 at pH 1, (E) 600 mM NaCl at pH 3, (F) 200 mM $CaCl_2$ at pH 3, and (G) 200 mM $ZnCl_2$ at pH 3.

tryptic digestion was applied as a simplified proteolysis model and used as a preliminary screening tool for protein stability and micronutrient release; while it is a widely accepted enzymatic model due to its defined cleavage specificity, the results cannot be extrapolated to the complexity of gastrointestinal digestion. In the undigested WPI samples, distinct bands appeared between 15 – 20 kDa and 1–10 kDa, corresponding to β-Lg (18.4 kDa) and α-LA (14.2 kDa), respectively (Fig. 5A), consistent with previous reports by Lorenzen and Schrader (2006). Additional bands appeared between 50 and 75 kDa, likely attributed to BSA with 66.5 kDa. Following trypsin digestion, the WPI samples exhibited similar band patterns, but with reduced intensity, indicating proteolytic degradation. Notably, β-Lg underwent more extensive degradation than α-LA. Moreover, the diminished intensity of the β-Lg and α-LA bands was accompanied by the appearance of several diffuse bands below 10 kDa, indicative of peptide formation through enzymatic hydrolysis, as also previously reported by Pintado and Malcata (2000) and Creamer et al.

(2004).

Digested WPI-based aerogels obtained from pH 1 solutions showed a more pronounced reduction in the β-Lg and α-LA bands compared to the digested WPI control (Fig. 5B–D). This reduction suggests enhanced digestibility, likely due to partial structural unfolding during aerogel formation, as also indicated by FTIR analysis, improving enzyme accessibility to cleavage sites and promotes hydrolysis. Correspondingly, the digested aerogels displayed stronger peptide bands below 10 kDa than the digested WPI. These observations align with findings described by Kananen et al. (2000), who noted increased resistance to trypsin in native whey proteins, as well as Kleemann et al. (2020) and Plazzotta et al. (2022), who confirmed the high digestibility of whey protein aerogels under intestinal conditions. Furthermore, at pH 1, aerogels containing calcium or zinc exhibited more pronounced digestion compared to those with sodium (Fig. 5C, D vs. Fig. 5B), implying a pronounced effect of divalent ions on proteolytic susceptibility. This effect likely reflects that divalent ions alter the protein network, thereby promoting local unfolding or structural rearrangements that increase enzyme accessibility and thus enhance proteolytic susceptibility (cf. Section 3.2 and 3.3).

In aerogels obtained from solutions at pH 3, trypsin digestion still resulted in a decrease of β-Lg and α-LA band intensities in the aerogels compared to the WPI control. Peptide bands below 10 kDa remain visible, indicating that partial hydrolysis has occurred. However, the overall extent of proteolysis was less pronounced in aerogels prepared at pH 3 than at pH 1, suggesting that more acidic conditions enhanced tryptic protein degradation; this was particularly evident from the lower intensity of bands at lower molecular weights. This reduced digestibility at pH 3 may be attributed to the compact packing of protein aggregates within the aerogel structure, as discussed in Section 3.3. This explanation aligns with findings described by Babaei et al. (2022), who reported that gels with densely packed networks hinder enzyme diffusion and limit access to cleavage sites within the gel matrix, thereby reducing the extent of proteolysis. Additionally, the type of ion present in the aerogels appears to have minimal influence on digestibility at pH 3, reinforcing the potential of these aerogels as functional carriers, regardless of the ionic composition. Furthermore, no reduction in trypsin activity was observed across different ion treatments, indicating that the presence of divalent cations did not inhibit enzymatic function (data not shown). Overall, these results demonstrate that pH and consequently, the associated structural density of the aerogels primarily influences their digestibility, while ion composition plays a minor role.

In order to assess zinc bioavailability, trypsin-digested and buffer-treated aerogel samples were applied to Caco-2 cells. Alterations in intracellular zinc levels were detected with the low molecular weight fluorescence sensor Zinpyr-1 (Fig. 6). Incubations were carried out with zinc at a concentration of 10 μM from either the zinc-aerogel samples or inorganic zinc salts ($ZnCl_2$ and $ZnSO_4$) as reference. This concentration mirrors what would be expected in the intestinal lumen after an average intake of dietary zinc (Cragg et al., 2002; Haase et al., 2020). The increase observed in Zinpyr-1 fluorescence upon $ZnCl_2$ or $ZnSO_4$ treatment aligns with findings from prior research in Caco-2 enterocytes (Maares et al., 2018b; Sauer et al., 2017). The combination of 1 % w/v WPI and 10 μM $ZnSO_4$ did not lead to a notable additional increase in Zinpyr-1 fluorescence. These results oppose the results reported by Li et al. (2022), who showed that β-Lg-bound zinc achieved twice the zinc delivery to 3D-cultured intestinal cells as $ZnSO_4$. Under the conditions of our experiment, the expected advantages of whey protein-zinc complexes in enhancing zinc (Li et al., 2022; Tang & Skibsted, 2016), did either not manifest or remained undetectable by fluorimetric analysis.

For the undigested zinc-aerogel samples, zinc transfer into Caco-2 enterocytes seemed to be reduced. A quenching effect from the aerogels is not a plausible explanation, as Zinpyr-1 fluorescence was similar in the cells from the control and the Na-aerogel treatments. The FTIR results suggest that the WPI proteins undergo certain structural changes during aerogel formation (Fig. 3). This could result in zinc being more firmly incorporated into the WPI aerogel matrix, potentially reducing its release. Still, a substantial fraction of the zinc from the undigested zinc-containing aerogels remained accessible for cellular uptake, probably via the Caco-2 microvillar transporters SLC39A4 (ZIP4), SLC30A5 (ZnT5 variant B) or SLC11A2 (DMT1) (Hall & King, 2023; Maares & Haase, 2020). Pre-digestion with trypsin caused a slight (but not statistically significant) upward trend in Zinpyr-1 fluorescence, for either WPI/$ZnSO_4$ co-incubation as well as the zinc-aerogels. It should be noted that digestion was not included as a factor in the *two-way* ANOVA, so the effect of pre-digestion is not fully captured in the statistical analysis. An explanation for the trend of higher intracellular zinc levels could be the formation of Zn-peptide chelates, which may support zinc delivery to Caco-2 cells through endocytosis following the assumptions described by Lin et al. (2024) or as recently proposed by Wang et al. (2023), via

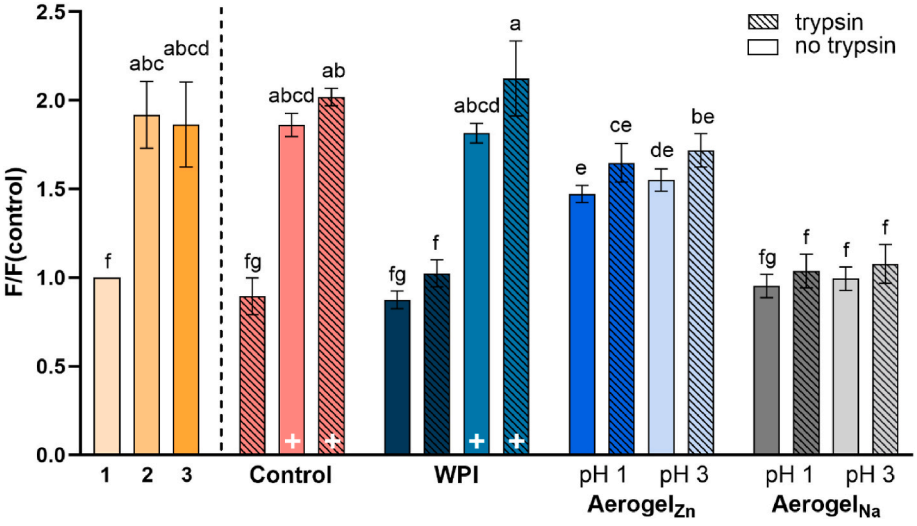

Fig. 6. Zinpyr1-fluorescence ratios indicating intracellular zinc levels in Caco-2 cells under various conditions. Caco-2 cells were included in all control and sample conditions. Controls include (1) buffer only, (2) 10 μM inorganic $ZnSO_4$ and (3) 10 μM inorganic $ZnCl_2$. Samples include digested and undigested matrices (without whey protein isolate (WPI) or aerogel) as well as WPI, with (+) and without addition of 10 μM $ZnCl_2$. Additionally, cell-containing samples with $ZnCl_2$-containing (final amount of 10 μM $ZnCl_2$) and NaCl-containing aerogels, prepared at pH 1 or pH 3, were tested in both undigested and digested form. Means that differ with statistical significance do not share the same letters and error bars represent standard deviation (*two-way* ANOVA, pH x ions, $p \leq 0.05$).

PepT1-mediated mechanisms. Any remaining intact whey proteins in the proteolytic digested aerogel samples (Fig. 5) likely interfered with the action of tryptic peptides, thereby diminishing their increasing effect on zinc absorption.

Taken together, the intrinsic properties of whey protein, its digestibility and potential to form zinc-binding peptides, highlight its value not only as a structural matrix but also as a functional carrier for controlled zinc delivery, especially in the intestinal environment. Moreover, it should be noted that the difference in zinc concentrations between the digestibility and Caco-2 assays limits the ability to directly correlate zinc release by proteolysis with cellular zinc uptake, and conclusions regarding their relationship should be interpreted accordingly.

3.5. Limitations

The study bears some limitations due to its model character. It was not designed for product development, but to assess the ability of protein-based aerogels to act as carriers for zinc provision. One of the considerable limitations is the absence of a salt-free WPI aerogel control. The NaCl-containing aerogel served as the closest internal reference, and comparisons were made with previously reported salt-free aerogels in the literature. However, a direct comparison within the present experimental framework could not be included. Another limitation concerns the structural characterization during aerogel preparation. Structural changes were only assessed at the beginning and at the end of the process, which does not provide the course of the conformational transitions. Nonetheless, these endpoint data capture the relevant states that determine zinc incorporation and release capacity. A further point relates to the morphological analyses. BET measurements, in particular, showed relatively high standard deviations. While this reduces the precision of quantitative conclusions, such variability is inherent to protein-based aerogels and reflects the structural heterogeneity of these materials rather than experimental variations. For the *in vitro* digestion experiments only trypsin was employed. However, tryptic hydrolysis is providing a defined, well-established and reproducible, but simplified, proteolysis model. This approach is widely used in protein research to screen for proteolytic stability and cleavage behavior, and it reveals general estimates of zinc-protein interactions. However, it does not represent the full enzymatic and physicochemical complexity of gastrointestinal digestion, which further involves multiple proteases, varying pH conditions, bile acids, additional cofactors, but mainly the co-ingestion of e.g., dietary constituents, often referred to as the 'food matrix'. Moreover, gastrointestinal processes are subject to interindividual variability (of the consumer), so the results of a single-enzyme model must be interpreted as indicative rather than representative. In the statistical evaluation of Caco-2 uptake data, digestion was not included as a factor in the *two-way* ANOVA. Consequently, the effect of pre-digestion is only partially represented in the analysis, and the results should be interpreted with this constraint in mind. Finally, differences in zinc concentrations between the digestibility assays and the Caco-2 experiments preclude direct correlation of proteolysis and cellular uptake. This reflects a necessary compromise in the experimental setup, as zinc levels in the Caco-2 assays had to be kept low and uniform across all conditions to ensure cell viability and comparability.

4. Conclusion

This study represents a first step toward understanding the potential of WPI-based aerogels as carriers for micronutrients such as zinc, by combining structural and morphological characterization with analyses of digestibility and zinc release in an intestinal model. Ion retention within the aerogels was influenced by both ion type and structural changes during aerogel formation. Although substantial losses occurred, aerogels prepared at pH 3 retained more ions, likely due to the protonation state of amino acid residues and the formation of a denser protein matrix compared to the more open structure at pH 1. Taken together with literature on no-salt-added protein aerogels, our results emphasize that protein aerogels can be tailored across a wide structural spectrum, from highly porous, salt-free matrices to denser, ion-coordinated networks with distinct functionalities.

The denser matrix obtained in this work reduced digestibility by limiting tryptic degradation, whereas aerogels formed at pH 1 showed enhanced enzymatic breakdown, particularly in the presence of divalent ions. Zinc release from all aerogels, however, appeared to be governed primarily by diffusion rather than enzymatic degradation. While zinc uptake was observed in Caco-2 cells, levels remained consistently lower than with free ZnCl2, indicating that the aerogel matrix did not enhance zinc bioaccessibility compared to the inorganic form.

This work advances previous studies by jointly considering structural modifications, digestibility, and zinc bioavailability in Caco-2 cells, providing a more holistic view of how protein-based aerogels may function in vivo. Future investigations should optimize release profiles under physiological conditions, assess stability and effects on organs and gut microbiota, and explore co-delivery of multiple bioactive compounds, including strategies to improve zinc retention. Long-term in vivo studies will be critical to establish safety and biological impact, while the influence of enzymes beyond trypsin warrants further study to clarify digestion and release mechanisms in more complex environments. As the present digestion experiments were based solely on trypsin as a simplified proteolysis model, and future work should extend to more comprehensive gastrointestinal simulations.

CRediT authorship contribution statement

Helena Kieserling: Writing – review & editing, Writing – original draft, Visualization, Validation, Supervision, Project administration, Investigation, Data curation, Conceptualization. **Jonathan Heine:** Writing – review & editing, Visualization, Investigation, Formal analysis, Data curation. **Baldur Schroeter:** Writing – review & editing, Visualization, Supervision, Methodology, Investigation, Data curation, Conceptualization. **Stephan Drusch:** Writing – review & editing, Supervision, Resources, Methodology. **Maria Maares:** Writing – review & editing, Writing – original draft, Supervision, Resources, Methodology, Data curation. **Sascha Rohn:** Writing – review & editing, Supervision, Resources. **Hajo Haase:** Writing – review & editing, Supervision, Resources, Methodology. **Pavel Gurikov:** Writing – review & editing, Supervision, Resources, Project administration, Methodology, Investigation, Data curation, Conceptualization. **Claudia Keil:** Writing – review & editing, Writing – original draft, Validation, Supervision, Project administration, Investigation, Data curation, Conceptualization.

Declaration of competing interest

The authors declare that they have no known competing financial interests or personal relationships that could have appeared to influence the work reported in this paper.

Acknowledgments

The authors would like to thank Mr. Dennis Thurack (University of Potsdam, Potsdam, Germany) for technical assistance with the LC-MS analysis. Peptide standards for LC-MS analysis were kindly provided by the Max-Rubner-Institute (Karlsruhe, Germany).

Data availability

Data will be made available on request.

References

Ahmadi, M., Madadlou, A., & Saboury, A. A. (2016). Whey protein aerogel as blended with cellulose crystalline particles or loaded with fish oil. *Food Chemistry, 196*, 1016–1022. https://doi.org/10.1016/j.foodchem.2015.10.031

Andlinger, D. J., Bornkeßel, A. C., Jung, I., Schröter, B., Smirnova, I., & Kulozik, U. (2021). Microstructures of potato protein hydrogels and aerogels produced by thermal crosslinking and supercritical drying. *Food Hydrocolloids, 112*, Article 106305. https://doi.org/10.1016/j.foodhyd.2020.106305

Andlinger, D. J., Schlemmer, L., Jung, I., Schroeter, B., Smirnova, I., & Kulozik, U. (2022). Hydro- and aerogels from ethanolic potato and whey protein solutions: Influence of temperature and ethanol concentration on viscoelastic properties, protein interactions, and microstructure. *Food Hydrocolloids, 125*, Article 107424. https://doi.org/10.1016/j.foodhyd.2021.107424

Babaei, J., Khodaiyan, F., Mohammadian, M., & Sheikhi, M. (2022). In vitro digestibility and functional attributes of the whey protein heat-induced hydrogels reinforced by various polysaccharides and CaCl2. *Journal of Food Measurement and Characterization, 16*(1), 19–28. https://doi.org/10.1007/s11694-021-01142-y

Betz, M., García-González, C. A., Subrahmanyam, R. P., Smirnova, I., & Kulozik, U. (2012). Preparation of novel whey protein-based aerogels as drug carriers for life science applications. *The Journal of Supercritical Fluids, 72*, 111–119. https://doi.org/10.1016/j.supflu.2012.08.019

Bryant, C. M., & McClements, D. J. (2000). Influence of NaCl and CaCl2 on cold-set gelation of heat-denatured whey protein. *Journal of Food Science, 65*(5), 801–804. https://doi.org/10.1111/j.1365-2621.2000.tb13590.x

Burdette, S. C., Walkup, G. K., Spingler, B., Tsien, R. Y., & Lippard, S. J. (2001). Fluorescent sensors for Zn2+ based on a fluorescein platform: Synthesis, properties and intracellular distribution. *Journal of the American Chemical Society, 123*(32), 7831–7841. https://doi.org/10.1021/ja010059l

Buszewski, B., Rodzik, A., Railean-Plugaru, V., Sprynskyy, M., & Pomastowski, P. (2020). A study of zinc ions immobilization by β-lactoglobulin. *Colloids and Surfaces A: Physicochemical and Engineering Aspects, 591*, Article 124443. https://doi.org/10.1016/j.colsurfa.2020.124443

Cao, X., Lee, H.-J., Shik Yun, H., & Koo, Y.-M. (2001). Solubilities of calcium and zinc lactate in water and water-ethanol mixture. *Korean Journal of Chemical Engineering, 18*(1), 133–135. https://doi.org/10.1007/BF02707210

Cragg, R. A., Christie, G. R., Phillips, S. R., Russi, R. M., Küry, S., Mathers, J. C., Taylor, P. M., & Ford, D. (2002). A novel zinc-regulated human zinc transporter, hZTL1, is localized to the enterocyte apical membrane. *Journal of Biological Chemistry, 277*(25), 22789–22797. https://doi.org/10.1074/jbc.M200577200

Creamer, L. K., Nilsson, H. C., Paulsson, M. A., Coker, C. J., Hill, J. P., & Jiménez-Flores, R. (2004). Effect of genetic variation on the tryptic hydrolysis of bovine β-lactoglobulin A, B, and C. *Journal of Dairy Science, 87*(12), 4023–4032. https://doi.org/10.3168/jds.S0022-0302(04)73543-2

Einhorn, V., Haase, H., & Maares, M. (2024). Interaction and competition for intestinal absorption by zinc, iron, copper, and manganese at the intestinal mucus layer. *Journal of Trace Elements in Medicine & Biology, 84, 127459*. https://doi.org/10.1016/j.jtemb.2024.127459

Fang, Y., & Dalgleish, D. (1997). Conformation of β-Lactoglobulin studied by FTIR: Effect of pH, temperature, and adsorption to the oil-water interface. *Journal of Colloid and Interface Science, 196*(2), 292–298. https://doi.org/10.1006/jcis.1997.5191

Fernández, A., & Riera, F. (2013). β-Lactoglobulin tryptic digestion: A model approach for peptide release. *Biochemical Engineering Journal, 70*, 88–96. https://doi.org/10.1016/j.bej.2012.10.001

FitzPatrick, S. E., Deb-Choudhury, S., Ranford, S., & Staiger, M. P. (2022). Canola protein aerogels via salt-induced gelation and supercritical carbon dioxide drying. *European Polymer Journal, 168, 111126*. https://doi.org/10.1016/j.eurpolymj.2022.111126

Gomis, V., Saquete, M. D., & García-Cano, J. (2013). CaSO4 solubility in water-ethanol mixtures in the presence of sodium chloride at 25°C. Application to a reverse osmosis process. *Fluid Phase Equilibria, 360*, 248–252. https://doi.org/10.1016/j.fluid.2013.09.063

Haase, H., Ellinger, S., Linseisen, J., Neuhäuser-Berthold, M., & Richter, M. (2020). Revised D-A-CH-reference values for the intake of zinc. *Journal of Trace Elements in Medicine & Biology, 61*, Article 126536. https://doi.org/10.1016/j.jtemb.2020.126536

Hall, A. G., & King, J. C. (2023). The molecular basis for zinc bioavailability. In *International journal of molecular sciences*. Multidisciplinary Digital Publishing Institute, 24 (7). https://doi.org/10.3390/ijms24076561.

Hao, J., Yuan, L., Zhu, Y., Bai, X., Ye, C., Jiao, Y., & Qiao, S. Z. (2023). Low-cost and non-flammable eutectic electrolytes for advanced Zn-I2 batteries. *Angewandte Chemie - International Edition, 62*(39). https://doi.org/10.1002/anie.202310284

Hoppenreijs, L. J. G., Brune, S. E., Biedendieck, R., Krull, R., Boom, R. M., & Keppler, J. K. (2023). Fibrillation of β-lactoglobulin at pH 2.0: Impact of cysteine substitution and disulfide bond reduction. *Food Hydrocolloids, 141, 108727*. https://doi.org/10.1016/j.foodhyd.2023.108727

Jackson, M., & Mantsch, H. (1995). The use and misuse of FTIR spectroscopy in the determination of protein structure. *Critical Reviews in Biochemistry and Molecular Biology, 30*(2), 95–120. https://doi.org/10.3109/10409239509085140

Jung, I., Schroeter, B., Plazzotta, S., De Berardinis, L., Smirnova, I., Gurikov, P., & Manzzocco, L. (2023). Oleogels from mesoporous whey and potato protein based aerogel microparticles: Influence of microstructural properties on oleogelation ability. *Food Hydrocolloids, 142*, Article 108758. https://doi.org/10.1016/j.foodhyd.2023.108758

Kallay, C., Varnagy, K., Micera, G., Sanna, D., & Sovago, I. (2005). Copper(II) complexes of oligopeptides containing aspartyl and glutamyl residues. Potentiometric and spectroscopic studies. *Journal of Inorganic Biochemistry, 99*, 1514–1525. https://doi.org/10.1016/j.jinorgbio.2005.04.009

Kananen, A., Savolainen, J., Mak, J., Perttilak, U., Myllykoski, L., & Pihlanto-Leppak, A. (2000). Influence of chemical modifcation of whey protein conformation on hydrolysis with pepsin and trypsin. *International Dairy Journal, 10*, 691–697. https://doi.org/10.1016/S0958-6946(00)00094-7

Kharlamova, A., Nicolai, T., & Chassenieux, C. (2020). Gelation of whey protein fractal aggregates induced by the interplay between added HCl, CaCl2 and NaCl. *International Dairy Journal, 111*, Article 104824. https://doi.org/10.1016/j.idairyj.2020.104824

Kieserling, H., Pankow, A., Keppler, J. K., Wagemans, A. M., & Drusch, S. (2021). Conformational state and charge determine the interfacial film formation and film stability of β-lactoglobulin. *Food Hydrocolloids, 114*, Article 106561. https://doi.org/10.1016/j.foodhyd.2020.106561

Kistler, S. S. (1931). Coherent expanded aerogels and jellies. *Nature, 127*(3211). https://doi.org/10.1038/127741a0, 741–741.

Kleemann, C., Schuster, R., Rosenecker, E., Selmer, I., Smirnova, I., & Kulozik, U. (2020). In-vitro-digestion and swelling kinetics of whey protein, egg white protein and sodium caseinate aerogels. *Food Hydrocolloids, 101*, Article 105534. https://doi.org/10.1016/j.foodhyd.2019.105534

Kleemann, C., Selmer, I., Smirnova, I., & Kulozik, U. (2018). Tailor made protein based aerogel particles from egg white protein, whey protein isolate and sodium caseinate: Influence of the preceding hydrogel characteristics. *Food Hydrocolloids, 83*, 365–374. https://doi.org/10.1016/j.foodhyd.2018.05.021

Kleemann, C., Zink, J., Selmer, I., Smirnova, I., & Kulozik, U. (2020). Effect of ethanol on the textural properties of whey protein and egg white protein hydrogels during water-ethanol solvent exchange. *Molecules, 25*(19). https://doi.org/10.3390/molecules25194417

Lefevre, T., & Subirade, M. (1999). Structural and interaction properties of ß-Lactoglobulin as studied by FTIR spectroscopy. *International Journal of Food Science and Technology, 34*(5–6), 419–428. https://doi.org/10.1046/j.1365-2621.1999.00311.x

Leite, A. C., Pereira, R. N., & Rodrigues, R. M. (2025). Protein aerogels as food-grade delivery systems - A comprehensive review. *Food Hydrocolloids, 163*, Article 111138. https://doi.org/10.1016/j.foodhyd.2025.111138

Li, T., Jiao, R., Ma, J., Zang, J., Zhao, G., & Zhang, T. (2022). Zinc binding strength of proteins dominants zinc uptake in Caco-2 cells. *RSC Advances, 12*(33), 21122–21128. https://doi.org/10.1039/d2ra03565k

Liang, X., Ma, C., Yan, X., Zeng, H., McClements, D. J., Liu, X., & Liu, F. (2020). Structure, rheology and functionality of whey protein emulsion gels: Effects of double cross-linking with transglutaminase and calcium ions. *Food Hydrocolloids, 102*, Article 105569. https://doi.org/10.1016/j.foodhyd.2019.105569

Lin, S., Li, J., Hu, X., Chen, S., Huang, H., Wu, Y., & Li, Z. (2024). Zn2+ chelating peptide GFLGSP: Characterization of structure/Zn2+ chelating mode and the potential mechanisms for promoting Zn2+ transport in Caco-2 cells. *Food Research International, 192*, Article 114829. https://doi.org/10.1016/j.foodres.2024.114829

Liu, X., Wang, Z., Yin, F., Liu, Y., Qin, N., Nakamura, Y., Shahidi, F., Yu, C., Zhou, D., & Zhu, B. (2019). Zinc-chelating mechanism of sea cucumber (Stichopus japonicus)-derived synthetic peptides. *Marine Drugs, 17*(438). https://doi.org/10.3390/md17080438

Liu, T., Zou, L., Ji, X., & Xiao, G. (2022). Chicken skin-derived collagen peptides chelated zinc promotes zinc absorption and represses tumor growth and invasion in vivo by suppressing autophagy. *Frontiers in Nutrition, 9*, Article 960926. https://doi.org/10.3389/fnut.2022.960926

Lorenzen, P. C., & Schrader, K. (2006). A comparative study of the gelation properties of whey protein concentrate and whey protein isolate. *Le Lait, 86*(4), 259–271. https://doi.org/10.1051/lait:2006008

Lovskaya, D., Bezchasnyuk, A., Mochalova, M., Tsygankov, P., Lebedev, A., Zorkina, Y., Zubkov, E., Ochneva, A., Gurina, O., Silantyev, A., Majouga, A., & Menshutina, N. (2022). Preparation of protein aerogel particles for the development of innovative drug delivery systems. *Gels, 8*(765). https://doi.org/10.3390/gels8120765

Lowe, N. M., Hall, A. G., Broadley, M. R., Foley, J., Boy, E., & Bhutta, Z. A. (2024). Preventing and controlling zinc deficiency across the life course: A call to action. *Advances in Nutrition, 15*(3), Article 100181. https://doi.org/10.1016/j.advnut.2024.100181

Maares, M., Duman, A., Keil, C., Schwerdtle, T., & Haase, H. (2018). The impact of apical and basolateral albumin on intestinal zinc resorption in the Caco-2/HT-29-MTX co-culture model. *Metallomics, 10*(7), 979–991. https://doi.org/10.1039/c8mt00064f

Maares, M., & Haase, H. (2020). A guide to human zinc absorption: General overview and recent advances of in vitro intestinal models. *Nutrients, 12*(762). https://doi.org/10.3390/nu12030762

Maares, M., Keil, C., Thomsen, S., Günzel, D., Wiesner, B., & Haase, H. (2018). Characterization of Caco-2 cells stably expressing the protein-based zinc probe eCalwy-5 as a model system for investigating intestinal zinc transport. *Journal of Trace Elements in Medicine & Biology, 49*, 296–304. https://doi.org/10.1016/j.jtemb.2018.01.004

Manzocco, L., Plazzotta, S., Powell, J., de Vries, A., Rousseau, D., & Calligaris, S. (2021). Structural characterisation and sorption capability of whey protein aerogels obtained by freeze-drying or supercritical drying. *Food Hydrocolloids, 122*, Article 107117. https://doi.org/10.1016/j.foodhyd.2021.107117

Maret, W. (2017). Zinc in cellular regulation: The nature and significance of "zinc signals.". *International Journal of Molecular Sciences, 18*(2285). https://doi.org/10.3390/ijms18112285

Mezzenga, R., & Fischer, P. (2013). The self-assembly, aggregation and phase transitions of food protein systems in one, two and three dimensions. *Reports on Progress in Physics, 76*(4). https://doi.org/10.1088/0034-4885/76/4/046601

Mottola, S., Cardea, S., Montella, F., Scognamiglio, M., Öztop, M. H., De Marco, I., & Ersus, S. (2025). Aerogels based on proteins extracted from plant sources: Different production methodologies. *Food and Bioproducts Processing, 151*, 148–157. https://doi.org/10.1016/j.fbp.2025.03.011

Nicolai, T. (2019). Gelation of food protein-protein mixtures. *Advances in Colloid and Interface Science, 270*, 147–164. https://doi.org/10.1016/j.cis.2019.06.006

Nicolai, T., Britten, M., & Schmitt, C. (2011). β-Lactoglobulin and WPI aggregates: Formation, structure and applications. *Food Hydrocolloids, 25*(8), 1945–1962. https://doi.org/10.1016/j.foodhyd.2011.02.006

Niu, Y., Xia, Q., Li, N., Wang, Z., & (Lucy) Yu, L. (2019). Gelling and bile acid binding properties of gelatin-alginate gels with interpenetrating polymer networks by double cross-linking. *Food Chemistry, 270*, 223–228. https://doi.org/10.1016/j.foodchem.2018.07.105

Peng, M., Lu, D., Yu, M., Jiang, B., & Chen, J. (2022). Identification of zinc-chelating pumpkin seed (Cucurbita pepo L.) peptides and in vitro transport of peptide–zinc chelates. *Journal of Food Science, 87*(5), 2048–2057. https://doi.org/10.1111/1750-3841.16132

Pintado, M. E., & Malcata, F. X. (2000). Hydrolysis of ovine, caprine and bovine whey proteins by trypsin and pepsin. *Bioprocess Engineering, 23*, 275–282.

Plazzotta, S., Alongi, M., De Berardinis, L., Melchior, S., Calligaris, S., & Manzocco, L. (2022). Steering protein and lipid digestibility by oleogelation with protein aerogels. *Food & Function, 13*(20), 10601–10609. https://doi.org/10.1039/d2fo01257j

Plazzotta, S., Calligaris, S., & Manzocco, L. (2020). Structural characterization of oleogels from whey protein aerogel particles. *Food Research International, 132*, Article 109009. https://doi.org/10.1016/j.foodres.2020.109099

Plazzotta, S., Jung, I., Schroeter, B., Subrahmanyam, R. P., Smirnova, I., Calligaris, S., Gurikov, P., & Manzocco, L. (2021). Conversion of whey protein aerogel particles into oleogels: Effect of oil type on structural features. *Polymers, 13*(23). https://doi.org/10.3390/polym13234063

Rink, L., & Gabriel, P. (2000). Zinc and the immune system. *Proceedings of the Nutrition Society, 59*(4), 541–552. https://doi.org/10.1017/S0029665100000781

Rodrigues, R. M., Martins, A. J., Ramos, O. L., Malcata, F. X., Teixeira, J. A., Vicente, A. A., & Pereira, R. N. (2015). Influence of moderate electric fields on gelation of whey protein isolate. *Food Hydrocolloids, 43*, 329–339. https://doi.org/10.1016/j.foodhyd.2014.06.002

Rodzik, A., Pomastowski, P., Sagandykova, G. N., & Buszewski, B. (2020). Interactions of whey proteins with metal ions. *International Journal of Molecular Sciences, 21*(6), 1–26. https://doi.org/10.3390/ijms21062156

Sauer, A. K., Pfaender, S., Hagmeyer, S., Tarana, L., Mattes, A. K., Briel, F., Küry, S., Boeckers, T. M., & Grabrucker, A. M. (2017). Characterization of zinc amino acid complexes for zinc delivery in vitro using Caco-2 cells and enterocytes from hiPSC. *Biometals, 30*(5), 643–661. https://doi.org/10.1007/s10534-017-0033-y

Sawyer, L., & Kontopidis, G. (2000). The core lipocalin, bovine β-lactoglobulin. *Biochimica et Biophysica Acta (BBA) - Protein Structure and Molecular Enzymology, 1482*(1–2), 136–148. https://doi.org/10.1016/S0167-4838(00)00160-6

Schroeter, B., Jung, I., Bauer, K., Gurikov, P., & Smirnova, I. (2021). Hydrophobic modification of biopolymer aerogels by cold plasma coating. *Polymers, 13*(17). https://doi.org/10.3390/polym13173000

Selmer, I., Kleemann, C., Kulozik, U., Heinrich, S., & Smirnova, I. (2015). Development of egg white protein aerogels as new matrix material for microencapsulation in food. *The Journal of Supercritical Fluids, 106*, 42–49. https://doi.org/10.1016/j.supflu.2015.05.023

Selvasekaran, P., & Chidambaram, R. (2021). Food-grade aerogels obtained from polysaccharides, proteins, and seed mucilages: Role as a carrier matrix of functional food ingredients. *Trends in Food Science and Technology, 112*, 455–470. https://doi.org/10.1016/j.tifs.2021.04.021

Si, K., Gong, T., Ding, S., Liu, H., Shi, S., Tu, J., Zhu, L., Song, L., Song, L., & Zhang, X. (2023). Binding mechanism and bioavailability of a novel phosvitin phosphopeptide (Glu-Asp-Asp-pSer-pSer) calcium complex. *Food Chemistry, 404*, Article 134567. https://doi.org/10.1016/j.foodchem.2022.134567

Smirnova, I., & Gurikov, P. (2018). Aerogel production: Current status, research directions, and future opportunities. *The Journal of Supercritical Fluids, 134*, 228–233. https://doi.org/10.1016/j.supflu.2017.12.037

Tang, N., & Skibsted, L. H. (2016). Zinc bioavailability from whey. Enthalpy-entropy compensation in protein binding. *Food Research International, 89*, 749–755. https://doi.org/10.1016/j.foodres.2016.10.002

Tolkach, A., & Kulozik, U. (2007). Reaction kinetic pathway of reversible and irreversible thermal denaturation of β-lactoglobulin. *Le Lait, 87*, 301–315. https://doi.org/10.1051/lait:2007012

Udechukwu, M. C., Downey, B., & Udenigwe, C. C. (2018). Influence of structural and surface properties of whey-derived peptides on zinc-chelating capacity, and in vitro gastric stability and bioaccessibility of the zinc-peptide complexes. *Food Chemistry, 240*, 1227–1232. https://doi.org/10.1016/j.foodchem.2017.08.063

von Oesen, T., Treblin, M., Clawin-Rädecker, I., Martin, D., Maul, R., Hoffmann, W., Schrader, K., Wegner, B., Bode, K., Zink, R., Rohn, S., & Fritsche, J. (2023). Identification of marker peptides for the whey protein quantification in edam-type cheese. *Foods, 12*(10). https://doi.org/10.3390/foods12102002

Wang, J., Li, X., McClements, D. J., Ji, H., Jin, Z., & Qiu, C. (2024). Preparation of protein-based aerogels and regulation and application of their absorption properties: A review. *Critical Reviews in Food Science and Nutrition, 65*(28), 5995–6011. https://doi.org/10.1080/10408398.2024.2434964

Wang, J., Niu, J., Ji, H., Li, X., McClements, D. J., Jin, Z., Jiang, L., Wen, J., & Qiu, C. (2024). Regulation of adsorption properties of Whey protein isolate fibril-calcium alginate aerogels by controlling protein fibrillation time. *Langmuir, 40*, 23230–23242. https://doi.org/10.1021/acs.langmuir.4c02474

Wang, B., Xiao, S., Zhou, G., & Wang, J. (2023). Novel casein-derived peptide-zinc chelate: Zinc chelation and transepithelial transport characteristics. *Journal of Agricultural and Food Chemistry, 71*(18), 6978–6986. https://doi.org/10.1021/acs.jafc.3c00001

Wang, R., Ye, M., Zhu, S., Zeng, Q., & Yuan, Y. (2023). Development, characterization and in vivo zinc absorption capacity of a novel soy meal hydrolysate-zinc complexes. *Frontiers in Nutrition, 10*, Article 1211609. https://doi.org/10.3389/fnut.2023.1211609

Wessells, K. R., & Brown, K. H. (2012). Estimating the global prevalence of zinc deficiency: Results based on zinc availability in national food supplies and the prevalence of stunting. *PLoS One, 7*(11). https://doi.org/10.1371/journal.pone.0050568

Yue, C., Ding, C., Su, J., & Cheng, B. (2022). Effect of copper and zinc ions on type I collagen self-assembly. *International Journal of Polymer Analysis and Characterization, 27*(6), 394–408. https://doi.org/10.1080/1023666X.2022.2093569